Screening wave conditions for the occurrence of green water events on sailing ships

van Essen, Sanne M.; Monroy, Charles; Shen, Zhirong; Helder, Joop; Kim, Dae Hyun; Seng, Sopheak; Ge, Zhongfu

DOI
10.1016/j.oceaneng.2021.109218

Publication date
2021

Document Version
Final published version

Published in
Ocean Engineering

Citation (APA)
van Essen, S. M., Monroy, C., Shen, Z., Helder, J., Kim, D. H., Seng, S., & Ge, Z. (2021). Screening wave conditions for the occurrence of green water events on sailing ships. *Ocean Engineering*, *234*, Article 109218. https://doi.org/10.1016/j.oceaneng.2021.109218

Ocean Engineering 234 (2021) 109218

Contents lists available at ScienceDirect

Ocean Engineering

journal homepage: www.elsevier.com/locate/oceaneng

Screening wave conditions for the occurrence of green water events on sailing ships

Sanne M. van Essen [a,d,*], Charles Monroy [b], Zhirong Shen [c], Joop Helder [a], Dae-Hyun Kim [c], Sopheak Seng [b], Zhongfu Ge [c]

[a] Maritime Research Institute Netherlands (MARIN), Wageningen, The Netherlands
[b] Bureau Veritas (BV) Marine & Offshore, Puteaux, France
[c] American Bureau of Shipping (ABS), Spring, TX, USA
[d] Delft University of Technology, Delft, The Netherlands

ARTICLE INFO

Keywords:
Screening
Critical events
Extreme events
Waves
Green water
Design loads
Multi-fidelity approach
Potential flow
Coarse mesh CFD

ABSTRACT

Design loads for extreme wave events on ships, such as slamming and green water, are hard to define. These events depend on details in the incoming waves, ship motions and structure layout, which requires high-fidelity tools such as CFD or experiments to obtain the correct loads. These tools (presently) do not have the capability to fully resolve the long-term statistics of rare events in all metocean conditions over the ship's lifetime. The idea of 'screening' is to use lower-fidelity numerical methods to identify the occurrence of extreme load events based on an indicator. A good indicator has a strong correlation to the design load, but is easier to calculate. A high-fidelity tool can then be used to find the loads in these events. The low-fidelity statistics and the high-fidelity loads can be combined to define a design load and its probability. The present study compares different numerical screening indicators for green water loads on a containership against experiments. The quality of the identification of the critical events and the required computational time served as comparison metrics. This showed that screening both with potential flow tools and with coarse mesh CFD tools is feasible, provided the indicator, grid, time step and wave input settings are well chosen. The results from coarse mesh CFD are slightly better than from potential flow, but the computational costs are much higher. The results also show that the peaks and steepness of the relative wave elevation around the bow are suitable green water load indicators, as well as the undisturbed wave crests at the bow. Fine mesh CFD calculations were done for the identified events based on an example indicator, which resulted in a green water load distribution very close to that of the experiments. This study shows that screening could potentially reduce the required high-fidelity modelling time with up to ~90% compared to common practice.

1. Introduction

1.1. Background and objectives

An important but hard to answer question for every ship design is how to handle extreme loading in waves, such as slamming and green water. More concretely: what should be the design green water load on a deck structure in the ship's operational profile? This is the topic of the present study by Cooperative Research Ships (CRS). Wave impact phenomena are highly non-linear (Johannessen and Hagen, 2012) and their loads depend on details in the flow, which means that they cannot be calculated with fast low-fidelity methods such as potential flow. Much progress has been made in recent years with high-fidelity modelling such as CFD and experiments. Good results were obtained with different types of CFD codes for extreme wave impacts on ships at zero speed (Pákozdi et al., 2014; Oger et al., 2014; Bandringa and Helder, 2018) and at forward speed (Nielsen, 2003; Kawamura et al., 2016; Ge et al., 2018). Air entrapments complicate such calculations (Bogaert, 2018; Scharnke, 2019), but their effect seems limited in green water impacts on deck structures (Buchner, 2002; van Essen et al., 2020b). Accurate fine mesh CFD results of the green water loads for the same case study as considered in the present publication were presented by Bandringa et al. (2020) (see Fig. 1). Still, present computational resources limit such detailed CFD calculations to a few 10–20 s events for the final ship design. Extreme events in waves are relatively rare, which makes obtaining their statistics challenging. On the one hand there is the long-term information about the metocean conditions in

* Corresponding author at: Maritime Research Institute Netherlands (MARIN), Wageningen, The Netherlands.
E-mail address: s.v.essen@marin.nl (S.M. van Essen).

https://doi.org/10.1016/j.oceaneng.2021.109218
Received 29 January 2021; Received in revised form 12 May 2021; Accepted 22 May 2021
Available online 7 June 2021

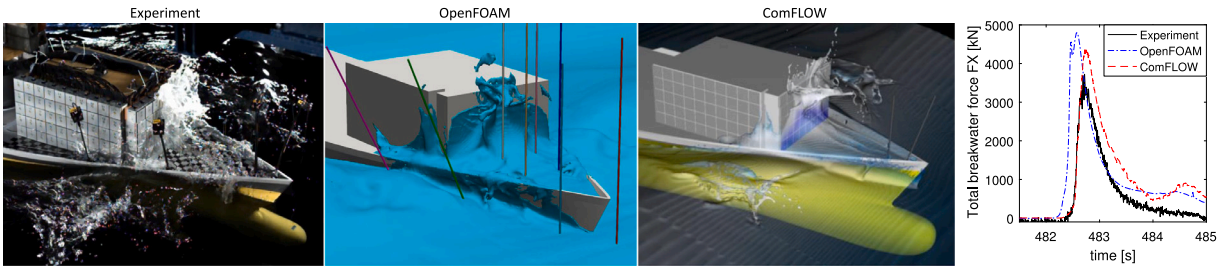

Fig. 1. Screenshot of green water event on the breakwater of the KCS containership and the total force on the breakwater from the experiments and from CFD codes ComFLOW and OpenFOAM, both CFD calculations on a fine mesh based on wave information and ship motions from the experiments (ComFLOW results described in detail in Bandringa et al., 2020 and van Essen et al., 2020b).

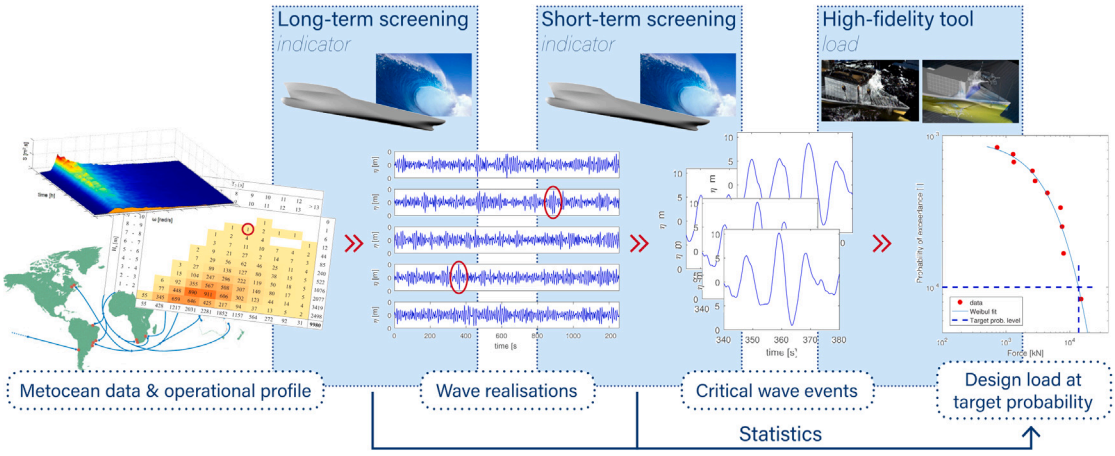

Fig. 2. Typical screening procedure, where the low-fidelity screening tool used to calculate a screening indicator can be e.g. a (non-linear) undisturbed wave code, potential flow code or CFD on a very coarse mesh. Indicator statistics can be obtained with these codes using Monte Carlo Simulation (MCS) or Response-Conditioning Methods (RCM).

the area of operation (wave scatter diagrams, wave spectra, wind and current conditions and operational data such as sailing route, sailing speeds and loading conditions), and on the other hand there is the high-fidelity modelling that typically has the capability to calculate loads over a few minutes. There is a need for a 'screening' procedure including tools with different levels of fidelity (and computational time) to help make the sea state and event selections. The following steps are distinguished (see also Fig. 2):

1. Define scatter diagrams for the operational profile.
2. Select critical sea states from the scatter diagram ('long-term screening').
3. Generate wave and response realisation time traces.
4. Select critical events in these time traces ('short-term screening').
5. Calculate the extreme loads for these events using a high-fidelity tool (CFD, model tests).
6. Use the loads from step 5 and the statistics from steps 2 and 4 to predict the long-term design loads and their probability.

Unfortunately, the highest wave crest does not always lead to the largest load. It is therefore often important to account for other wave and ship parameters. The idea is to use a fast 'screening' or 'surrogate' model for the selections of 2 and 4. Such a model should be able to calculate an indicator that has a strong relation to the critical load. An example of an indicator for green water could be relative wave elevation (RWE). If there is a fast tool that can calculate RWE reasonably accurately, this can be used to identify possibly critical green water events to run in a high-fidelity tool. The approach can in principle be used for any type of rare event in waves. In the present study, the green water loads on the breakwater of a container ship are used as case study. The objectives are to evaluate whether event selection based on a numerical indicator is feasible for this case, and if so, to find suitable tools and indicators. This validates short-term screening step 4 in the procedure. Some first results for step 5 and 6 are also provided. The study thus contributes towards an overall screening approach that could predict the design green water loads with a certain probability level, based on long-term wave information.

1.2. Review of earlier work

The first studies that explicitly mention screening were done when weakly non-linear time-domain seakeeping calculations were still computationally demanding. Linear screening was applied to find interesting occurrences of for instance global ship bending moments (Torhaug, 1996; Dietz, 2004). The increase of computational power and development of CFD in recent years makes screening potentially interesting for highly non-linear phenomena such as green water loading. Relevant literature can roughly be divided into three groups: (1) identification of suitable indicators for green water or slamming impacts (which are considered to be similar phenomena), (2) speeding up the screening using Response-Conditioning Methods (RCM) instead of Monte Carlo Simulations (MCS) and (3) the interaction between different levels of tools. Finally, the common practice for present designs is explained.

Indicators. Many studies focus on the details of green water or slamming impact loads, but the present study considers indicators that predict their occurrence. Hennig et al. (2015) showed strong effects on non-linear effects such as upwelling, non-linear waves and wave breaking on local slamming and airgap impact loads on platforms. Scharnke (2019) added that air entrapments and jets on the front of a deck box may lead to local variations in wave impact loads, but also showed that direct impacts dominate the loading process for the global impacts. This is promising for screening, as global flow is easier to solve with low-fidelity tools than local details. In 1964 already, Ochi (1964b) related relative vertical water velocity at a ship

bow to peak slamming loads and Ochi (1964a) showed that green water loads can be related to the static pressure of water on deck. Buchner (1994) showed that the forward speed of the ship causes a dynamic amplification of this pressure. Bales (1977) linked the occurrence of slamming and green water for a ship sailing in head seas to RWE, and showed that the influence of non-linearity in the incoming waves can be significant. Voogt and Buchner (2004) confirmed this effect of wave steepness on impacts. Ersdal and Kvitrud (2000) showed that the pitch motions of a ship as well as the memory effects in wave groups are important in the occurrence of green water events. Buchner (2002) developed an empirical method to determine green water loads, based on RWE and water height and velocity on deck. Ogawa et al. (2002) and van 't Veer and Vlasveld (2014) showed that non-linearity should be considered to estimate higher RWE on the bow of a ship, but also showed that the general trends of freeboard exceedance on a floating platform can be predicted using potential flow. This is promising for a screening application, where the exact predicted indicator value is less important than its relative ordering with respect to the green water load. Eggers et al. (2012) stated that the potential energy of the water flowing on deck is a better indicator to predict the green water loading on crew and deck structures of small and fast ships such as sailing yachts. Grin et al. (2013), Buchner et al. (2014) and van Essen et al. (2020a) showed that waves running up along the side of vessels could be used as indicator for green water impacts on structures on their side (such as overhanging lifeboats on cruise ships). Two types of impacts on a sailing ship were distinguished by Kapsenberg (2018): due to large ship motions and due to steep wave impacts. They may require different indicators, either related to ship motions (relative vertical bow motion or velocity) or to wave properties (steepness, crest kinematics). A number of studies identified experimental impact indicators: Stansberg (2008) defined an 'impact alert parameter' (based on undisturbed wave crest height, wave height, orbital velocity and steepness) to screen sea states for the occurrence of bow flare slamming and green water impacts on an FPSO deck house, Bunnik et al. (2018) showed that the RWE and its rise time may be good indicators to screen for wave impacts on both tension-leg and semi-submersible platforms, Bunnik et al. (2019) showed that the undisturbed wave crest height is a suitable indicator for wave-in-deck loads on a jacket platform and undisturbed wave steepness for impacts on a wind turbine, and finally (Stansberg, 2020) showed that the undisturbed vertical wave rise velocity is a good indicator for wave-in-deck loads on a gravity-based structure.

In summary, it seems that (non-)linear RWE, wave steepness and pitch motions could be indicators that predict the occurrence of green water loads on larger ships. Wave groups could also be considered as indicator. Variables describing the water flow (flux or kinematics) on or just in front of the deck may also be considered, if they can be calculated with a lower-fidelity tool.

Response-conditioning. These methods can be used to find a wave event, conditioned on a certain target response value or probability. This can be used to speed up screening compared to MCS. In this category, the Equivalent Design Wave (EDW) method conditions a regular wave based on a linear response transfer function. One step more complex, several methods are based on the 'New Wave' theory (Lindgren, 1970; Tromans et al., 1991). This provides an irregular Gaussian wave group profile based on the auto-correlation function of the wave spectrum, for a target response. Examples are the original theory (target wave crest amplitude), the Most Likely Wave (MLW) method (Friis-Hansen and Nielsen, 1995) (target wave crest amplitude and instantaneous frequency), the Most Likely Extreme Response (MLER) method (Adegeest et al., 1998) and its directional version (DMLER) (Pastoor, 2002) (target linear response amplitude and its mean frequency). The Most-Likely Response Wave (MLRW, or Conditioned Random Response Wave, CRRW) method (Dietz, 2004; Dietz et al., 2004; Taylor et al., 1997) generates a range of wave profile realisations for a target response amplitude and response frequency, by accounting for the random background of the sea state and response function. This means that it is no longer assumed that all wave components are in phase at the crest of the design wave, but have one of the phase realisations leading to the target response. When the target wave frequency is the mean wave frequency, the MLW and original New Wave profiles are identical. Similarly, when the target response frequency is the mean response frequency, the mean MLRW and the MLER wave profiles are identical. The aforementioned methods all condition the wave profile on a specific value for the response, usually the most probable maximum (MPM) for the given exposure duration. The Design Loads Generator (DLG) (Kim, 2012) and its non-linear response version NL-DLG (Seyffert, 2018) extend this to a probabilistic approach, finding a range of irregular linear wave events that fit the ensemble maximum response distribution for the given exposure duration. DLG can generate an ensemble of wave elevations that would produce the extreme value distribution of a target response for a given exposure period. This method was successfully applied to find the statistics of non-linear responses, such as whipping in head sea or parametric rolling in short-crested seaways (Kim et al., 2012; Kim and Troesch, 2014). While the approaches in Dietz et al. (2004) and Kim (2012) can account for parameters such as wave steepness and memory effects of ship motion in wave groups, these approaches have not been directly applied to the prediction of extreme green water impacts yet. Seyffert et al. (2020) compares MCS results for trimaran bending moments to results from DLG and modified versions of EDW and CRRW, showing that DLG provided the closest results to MCS.

All mentioned RCM techniques deliver linear Gaussian wave profiles, which may limit their applicability to highly non-linear events. However, they may be interesting to consider when a screening method based on linear wave input is selected.

Interaction fidelity levels. The use of screened events in a high-fidelity tool (step 4 to 5) is challenging due to the reduced-order wave modelling in most screening tools. A method to solve the problem of running a linear wave event in CFD is described by Johannessen and Lande (2018): the 'Event Matching' method. Events were selected based on an indicator in linear MCS. These events were matched to a database of fully non-linear wave events, after which the 'closest fit' non-linear event was run in CFD. This enables the inclusion of higher-order wave effects and wave breaking in the screening process. This importance of wave breaking in screening for wave-in-deck loads was confirmed by Bøckmann et al. (2018). However, this method is hard to apply when ship motions and forward speed are important. Alternatively, direct coupling methods such as applied in Pákozdi et al. (2014) could be used.

Common practice. In the offshore industry, the 'contour-line method' (Haver and Kleiven, 2004; Haver and Winterstein, 2008) is often used to derive long-term design loads for wave impacts. This approach uses general RCM method IFORM (inverse first-order reliability method Winterstein et al., 1993) to identify contour lines of equal joint sea state parameter probability (e.g. wave height and period), accounting for some short-term variability. The method equals the long-term probability of the response to the long-term probability of the sea state. The short-term probability of the response in a few identified sea states is then evaluated using many experimental wave realisations with a certain exposure duration (e.g. 3 h). This approach is commonly applied (e.g. DNV, 2010), but some of the assumptions are under debate. The approach disregards the contribution of long exposure times in relatively mild sea states to the failure probability (it favours short exposures of severe conditions), and it does not account for multi-modal failure due to different failure modes (Seyffert et al., 2021). Other limitations are the need to simplify the joint distribution of the environmental parameters, which may disregard complex interactions, and the assumption that sea states are independent (disregarding the influence of groupiness due to storms). The latter two limitations were improved in an alternative procedure based on hindcast data by Derbanne and de Hauteclocque (2019).

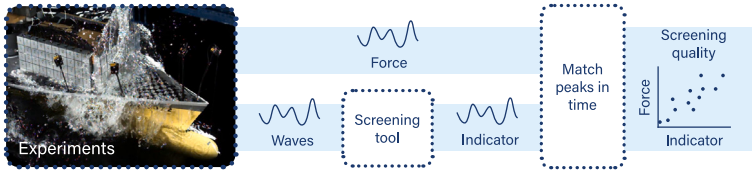

Fig. 3. Schematic approach of a large part of the present paper.

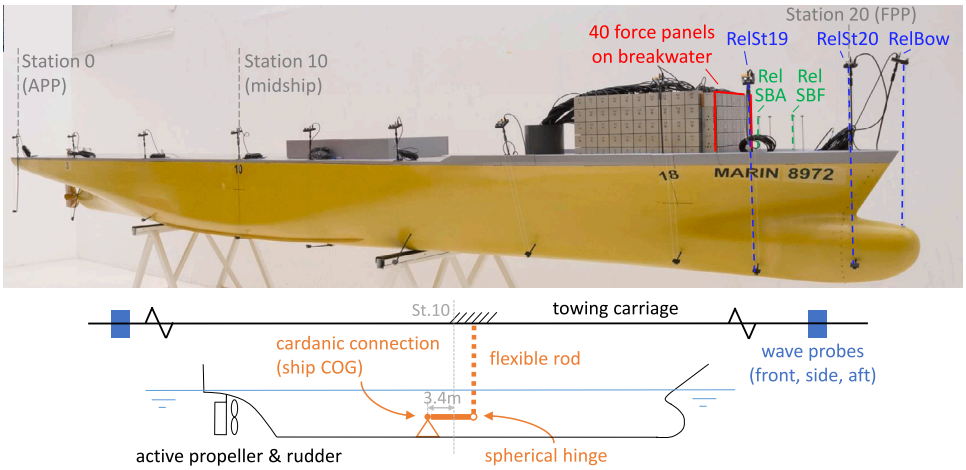

Fig. 4. KCS model and test set-up, with relative wave elevation probes and breakwater force panels, and a pole acting as spring in surge direction (free in the other degrees of freedom). Origin: APP, centreline, baseline.

1.3. Approach

Some of the aforementioned studies included numerical screening indicators, but usually only one or a few, and for weakly non-linear phenomena. Numerical indicators are required in practice, as experimental data is usually not available in an early design stage. The number of studies focussing on green water impacts on ships at speed is also limited. If screening methods are considered in earlier studies, they are usually fully linear (e.g. potential flow). This is logical, as long-term screening can only be done based on simplified models containing only the essential physics. However, for green water impacts it can be imagined that (some) wave non-linearity is essential to identify the correct critical events. The present study therefore compares the use of a large number of numerical screening indicators and tools to predict green water loads on a sailing ship, including validation with experiments and including some methods based on non-linear wave input. Green water events are rare, so very long duration experiments would be required to obtain converged statistical data. In order to enable validation based on limited-duration data, experiments were deterministically reproduced in the numerical tools instead. The downside of this approach is that it requires deterministic wave reproduction in the numerical tools, which is complicated. This is also addressed. As a direct deterministic comparison was used, MCS or RCM were not required in the present study.

Experiments were done with a containership, measuring the green water impact forces on a breakwater. Five different potential flow tools and three different CFD tools with a very coarse mesh were applied to calculate various green water indicators. The peaks in these indicators were then used to identify green water events, which were compared to the 'actual' experimentally measured events in order to validate them. The simplified validation procedure is shown in Fig. 3 — this is further explained in the following sections. The quality of the identification of the critical events in the wave realisation and the required computational time serve as comparison metrics. The speed of the computations is an important criterion, as large amounts of wave data need to be screened in an early design stage.

This publication is structured as follows: Section 2 describes the experiments and Section 3 the calculations. Section 4 explains some definitions and Section 5 shows the screening results and discussion. This includes a demonstration of the use of the identified events in a high-fidelity tool to predict the load distribution and a comparison to common practice. Finally, Section 6 draws some conclusions, and Section 7 discusses possible future work.

2. Experiments

Experiments were done with a scale 37.89 model of the KCS container ship (SIMMAN, 1997) (see Fig. 4). Its full-scale dimensions at the selected draught are L_{pp} 230 m, B 32.2 m, T 10.8 m with a freeboard at the bow of 7.4 m. All results in the present publication are provided at full scale. The tests were done in MARIN's Seakeeping and Manoeuvring Basin (SMB), measuring 170 × 40 × 5 m. The model was tested in a free-sailing set-up with its own active propulsion, consisting of a propeller at a fixed RPM and an active rudder. It was steered with an autopilot to keep its heading. A constant speed was required for the measurement carriage and the attached wave probes, for the deterministic numerical reproduction of the wave conditions (see Section 3). In order to enable this without 'losing' the model, the free-sailing set-up was combined with a cardanic pole set-up acting as spring in surge direction (surge stiffness of the system 6.5e3 kN/m, leading to a natural surge period of 18.9 s, see Fig. 4). The model surge speed varied due to the first-order wave excitation, but the second-order low-frequency speed variations were limited by the spring. All other ship motions (sway, heave, roll, pitch and yaw) were free. The model sailed in head and bow-quartering waves. In head waves, the measurement carriage did not move in y-direction. In bow-quartering waves, it followed the model in y-direction to account for the drift of the model. The roll period of the ship was adjusted to 27.5 s, such that it was far from wave encounter period in the tested conditions. This reduced the influence of roll motions on the occurrence of green water events.

The model was instrumented to measure the six degree of freedom ship motions, RWE at 11 locations along the weather side of the ship

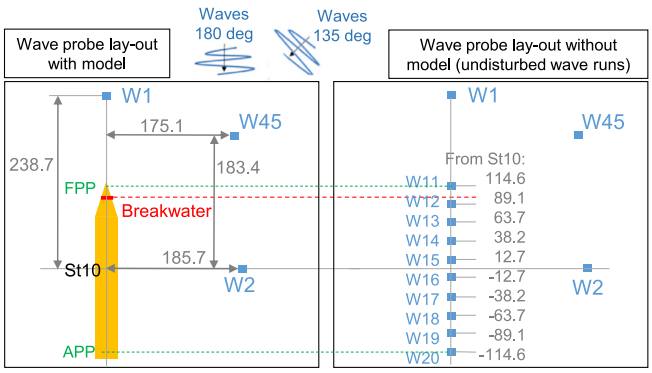

Fig. 5. Wave probe set-up with model at its rest position (left) and for undisturbed wave runs with extra probes over the ship centreline (right), where all wave probes W# were attached to the measurement carriage. Distances at full-scale in metres. W1,2,45 were at the same location with and without model. W1,2,45 were acoustic probes, W11-20 were resistance-type probes.

(where RelBow, RelSt20 and RelSt19 are used in present publication), RWE at 4 locations on the fore deck (RelSBA an RelSBF on starboard are used here), impact forces on 40 panels on the front of a breakwater and on 50 panels on the side of a container stack. Throughout this publication, results labelled as RelBow are the RWE results at probe RelBow. The locations of these sensors are indicated in Fig. 4. Only the force panels on the breakwater, at the front of the block on deck, are used in the present publication. They were placed in 5 rows of each 8 panels, at 16.0 m behind the forward perpendicular (FPP). Each force panel had a size of 1.89 × 1.89 m full-scale. The incoming waves around the ship were also measured at three locations, moving with the measurement carriage at a constant forward speed (see Fig. 5). Motions and incoming waves were measured at full-scale sample frequency 16.2 Hz, RWE at 32.5 Hz and forces at 780 or 1550 Hz.

The experimental conditions are listed in Table 1. The test conditions were determined such that a significant number of green water events occurred. The wave conditions are relatively steep. The vessel speeds were determined based on typical Class requirements in severe waves and the estimated maximum sustained speed of the KCS in wind and waves. Nine tests in irregular waves at forward speed were performed, each with a full-scale duration around three hours. The tests were performed in multiple consecutive runs (as the basin has a finite length), which were joined in the analysis. In each three-hour test, one run was selected (based on a large green water impact), to be deterministically repeated without model to measure the undisturbed waves.[1] For these runs, some additional wave probes were placed over the centreline of the model (see Fig. 5). Even though the wave generator and measurement carriage motions were accurately repeated, the repeatability of the wave condition in the basin is not perfect due to small wave-induced currents and wave breaking effects. This was discussed for the same experiments in van Essen (2019, 2021). Based on that work, the wave measurements with and without model were considered close enough to use the undisturbed waves as input for (some) deterministic calculations. Test 100504 is considered as example test in this publication. It consists of 6 runs with a total duration of 3:14 h. Its first run 10050401, with a duration of 0:30 h, is also used as example. This particular run was also repeated without model to measure the undisturbed waves (the other five runs were not).

[1] Naming convention: a 6-digit number indicates a full test (duration around 3 h) and a 8-digit number indicates one run (duration depending on vessel speed, either around 30 min at 5 kn or around 15 min at 10 kn). The run number is composed of the test number and two additional digits. Examples: test 100504 run 1 is also called run 10050401; test 100505 run 10 is also run 10050510.

Two groups of results were generated: for nine tests of three hours each, and for this single example 30 min run. They are abbreviated here as 3 h and 30 min, respectively.

3. Calculations

Different numerical codes were evaluated as screening tools, and each of these codes was used to derive a number of green water indicators. Several potential flow codes and CFD codes run on a coarse mesh were considered. The properties of all codes and the calculated indicators are described in the present section. The present study was based on calculations done by different project partners, who each used their best practice and insight to derive the indicators. It is therefore not a systematic study of all possible input variations, but a comparison of the inputs considered to be 'best practice' by each partner.

3.1. Potential flow

Different 'flavours' of potential flow tools are available, which differ in their handling of forward speed, motion (non-)linearity and wave (non-)linearity. First, forward speed: Rankine-source methods account correctly for forward speed in the source terms, whereas methods using zero speed Green's functions account only for forward speed in the encounter frequency corrections and the roll damping terms. Rankine-source codes are expected to better describe RWE at the bow, due to the prevention of unrealistic wave pile-up. The forward speed for the present study is low, so the differences were expected to be small. Both types of methods are included in the present study. Secondly, the codes differ in the level of (non-)linearity of the motion calculation. Linear and weakly non-linear Froude–Krylov methods are available. The latter methods account for some non-linearity in the ship motions, by using the 'actual' wetted area instead of the calm water wetted area in the calculation of the diffraction forces. The ship motions are limited for the 230 m ship in short and steep waves, but the Froude–Krylov terms may slightly improve the calculated indicators. Both types of methods are included in the present study. Finally, different choices can be made for the wave (non-)linearity. Most potential flow methods include linear input waves, but some account for second- or higher-order waves. However, most available non-linear wave potential flow methods only calculate undisturbed waves; they are not well validated and used for ship response (especially not at forward speed). This may be an option for the future. The use of 'wave-only' codes for screening may also be considered, if the ship motions are small. The wave non-linearity is expected to be more important than the ship motion non-linearity in the present steep wave conditions. Presently, only potential flow tools with linear wave input are included in the study. Of course there is also the difference in frequency- or time-domain codes, but as long as the described physics are the same, different results are not anticipated.

The following potential flow tools were applied by the Maritime Research Institute Netherlands (MARIN), Bureau Veritas (BV) and American Bureau of Shipping (ABS):

- HS: linear frequency-domain zero speed Greens function diffraction code Hydrostar, applied by BV;
- HS^{++}: weakly non-linear Froude–Krylov time-domain code Hydrostar^{++}, based on Hydrostar diffraction input, applied by BV;
- NL3: weakly non-linear Froude–Krylov time-domain code NLoad3D (ABS, 2013), based on Rankine-source diffraction input, applied by ABS;
- PRE: linear frequency-domain zero speed Greens function diffraction code PRECAL_R (developed by CRS), applied by MARIN;
- FAT: linear frequency-domain Rankine-source diffraction code FATIMA (Bunnik, 1999), applied by MARIN.

Table 1
Test programme, where μ = heading (180 deg head waves, 150 and 135 deg bow-quartering waves), H_s = significant wave height, T_p = peak wave period, V_x = mean forward speed, V_y = mean drift speed. All waves: long-crested JONSWAP wave spectrum with peak enhancement factor 3.3. 'Repeated runs' were without model to measure undisturbed waves. # wave encounters: zero up-crossing crests measured at probe W1.

Test no.	100501	100502	100505	100504	100506	100702	100705	100703	100704
# runs	6	12	6	6	6	6	6	7	12
Duration (s)	11 774	11 305	11 256	11 635	11 154	11 972	11 654	11 704	11 431
μ (deg)	180	180	180	180	180	150	150	135	135
H_s (m)	9.1	8.8	7.4	6.8	6.4	7.3	7.0	7.0	6.8
T_p (s)	11.2	11.2	12.1	9.7	12.1	11.2	9.7	9.7	9.7
V_x (kn)	5.0	10.1	5.0	5.0	5.0	5.0	5.0	5.0	10.1
V_y (kn)	0	0	0	0	0	0.73	0.5	0.92	0.75
# wave encounters	1337	1464	1301	1528	1312	1435	1533	1486	1661
Repeated run no.	10050105	10050202	10050510	10050401	10050602	10070201	10070502	10070302	10070413

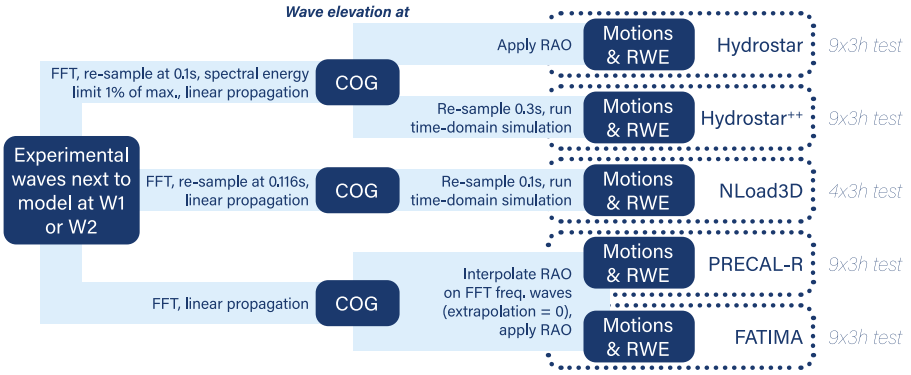

Fig. 6. Definition of wave input for the potential flow codes.

An overview of the applied code versions, properties and settings is provided in Appendix A. As explained in the introduction, the wave conditions have to be deterministically reproduced in the numerical tools. This is not straightforward, as the undisturbed waves at the required input locations are not directly available. Fig. 6 shows steps taken to define this wave input per code.

All considered potential flow methods require linear(ised) wave input at the ship centre of gravity (COG). Undisturbed wave repeat runs are not available for the full 3 h tests. This means that the waves have to be propagated to the ship COG based on wave measurements around the model. This was done using linear dispersion for all codes. Different wave probes can be selected to serve as basis for the propagation (Fig. 5). The difference in results between input based on probe W1 or W2 is only an issue in the validation study performed here. In a 'real' screening study there are still limitations due to the linear wave input in the potential flow codes, but not due to linear propagation from another location. The error introduced by the assumed linear wave propagation for relatively steep sea states in the screening validation study should therefore not affect the results more than necessary. The reference wave probe leading to the best match with the experiments was therefore selected for each test. This depends on different effects: propagation distance (shorter should be better, so errors larger from W1 than W2), diffracted waves from the model to the probe (larger at W2 than W1, and larger in bow-quartering waves than in head waves) and radiated waves from the model (larger at W2 than W1, and larger at higher speed). The input probe was therefore selected per test, based on the average correspondence of RWE and motions from all potential flow codes with the experiments. This led to selection of input wave probe W1 for all tests in bow-quartering waves and test 100502 in head waves at 10 kn speed, and probe W2 for all tests in head waves at 5 kn speed. The potential flow results in the remainder of this publication are all based on this choice. Fig. 6 shows that the project participants made different choices for the potential flow code wave input, which may partly determine the outcome. For HS and HS^{++}, a spectral energy limit was used at the input wave probe location, and the wave input was re-sampled. The NL3 wave input was also re-sampled. For PRE and FAT, the input waves were not changed. Instead, their response functions were interpolated at the wave FFT frequencies before applying them to the waves at the ship COG.

3.2. Coarse mesh CFD

Most CFD green water studies use one of the two major methods: grid-based Eulerian Navier–Stokes (NS) or particle-based Smoothed Particle Hydrodynamics (SPH). The grid-based methods have advanced greatly in recent years, to 3D simulation of green water loads on ships at speed in irregular waves (see e.g. Fig. 1). For the present 'coarse mesh' application, confidence in the grid refinement convergence characteristics of the CFD methods was required. There is sufficient experience with the grid-based methods to know approximately what to expect from coarse grids, whereas the experience with particle-based methods was not sufficient to know what to expect from coarsely distributed particle meshes. Only grid-based methods were therefore evaluated in the present study, also because this type of methods is relatively efficient. The following three coarse mesh finite volume CFD methods were applied to in order to calculate green water indicators:

- OFA and OFA1: unstructured grid finite-volume CFD method OpenFOAM, applied by ABS, using a dynamic overset grid technique (Shen and Korpus, 2015; Shen et al., 2016) and the wave2foam library for wave generation and absorption (Jacobsen et al., 2012). OFA was run for the 3 h test 100504 and OFA1 for the 30 min run 10050401 only, which also necessitates different wave input (this is further explained below);
- OFB: unstructured grid finite-volume CFD method OpenFOAM, applied by BV, using the foamStar library for wave generation and absorption (Benhamou et al., 2018);
- CF1,2,3: structured Cartesian-grid finite volume CFD method ComFLOW (Luppes et al., 2013), applied by MARIN. This was run on three different grids: grid 1 (coarse) to grid 3 (very coarse), for details see Table 7. The finest grid 1 was only run for the 2D wave

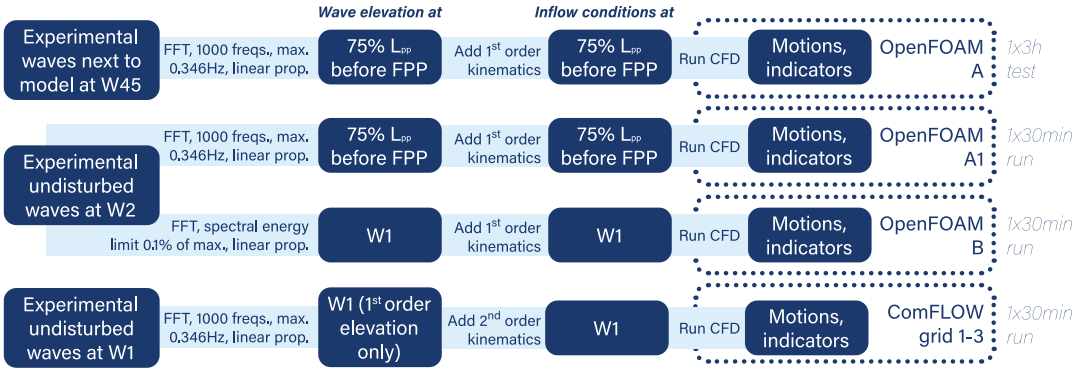

Fig. 7. Definition of wave input for the coarse mesh CFD codes.

Table 2
Numerical 'test programme' referring to the test numbers in Table 1, and evaluated indicators in the experiments and calculations. EXP = experiments, probe positions see Figs. 4 and 5.

Code	EXP	FAT	HS	HS^{++}	NL3	PRE	OFA	OFA1	OFB	CF1-3
Tests (v = tested or calculated 3 h condition)										
100504	v	v	v	v	v	v	v	run 1	run 1	run 1
100502, 100702, 100703	v	v	v	v	v	v	–	–	–	–
100501, 100505, 100506, 100705, 100704	v	v	v	v	–	v	–	–	–	–
Screening indicators (x = included indicator, L = derived indicator using linear dispersion)										
Crests + steepness undisturbed wave at W11	L	L	L	L	L	L	–	x	x	x
Peaks RWE at RelBow, RelSt20	x	x	x	x	x	x	x	x	x	x
Peaks RWE at RelSt19	x	x	x	x	x	x	x	x	–	–
Rise time + steepness RWE at RelBow	x	x	x	x	x	x	–	–	–	–
Peaks RWE at RelSBA, RelSBF	x	–	–	–	–	–	x	x	–	x
Troughs vertical bow position + velocity	x	x	x	x	x	x	x	x	x	x
Peaks coarse mesh FX total	–	–	–	–	–	–	x	x	x	x
Peaks coarse mesh FX per row of panels	–	–	–	–	–	–	x	x	–	x
Peaks flux through planes on deck	–	–	–	–	–	–	x	x	–	x

input; the other two grids both for the 2D wave input and the 3D simulations including model.

The coarse mesh simulations were done in two steps: 2D undisturbed wave propagation, and simulation on an equivalent 3D mesh including the ship. The CFD codes were only applied to tests in head waves, so 2D undisturbed wave results are sufficient. An overview of the applied code versions, properties and (grid and time step) settings is provided in Appendix A. The CFD codes need wave input at their defined inflow locations, which were defined at different locations in the different codes. Fig. 7 gives an overview of the steps taken to define this input.

This figure shows that different choices were made for the inflow location and the wave definition at this location. These differences have to be kept in mind, as they partly determine the outcome. All considered coarse mesh CFD codes were applied to the same 30 min run 10050401 (see next Section 3.3), for which there is an undisturbed wave repeat run available. ABS also applied OpenFOAM to full 3 h test 100504 (so to run 10050401 and five other runs), for which no undisturbed wave repeat run was available. OFA1 (for one run) and OFA (for six runs) therefore have a different wave input method. For the 3 h test with OFA, the waves at probe W45 with model were used as basis for the input, whereas for OFA1 the undisturbed waves at probe W2 were the basis for the input. In both cases, these waves were linearly propagated to the wave inflow location. OFB used a similar procedure as OFA1: linear propagation of the measured waves at one of the probe locations to the inflow location (after applying a spectral energy limit to the waves at the input wave probe). All three codes OFA, OFA1 and OFB added first-order wave kinematics to the thus defined wave elevation at the inflow location. CF1-3 used a different approach. The inflow was defined at probe location W1, such that the measured waves could directly be used as input without the need of propagation from another location. CF1-3 also used second-order wave kinematics (Sharma and Dean, 1979) at the inflow location, based on the first-order wave elevation (the measured wave elevation was split in first- and second-order components in order to do this following Stansberg, 1998; Buchner et al., 2007).

3.3. Calculation conditions and indicators

Table 2 shows the numerical 'test programme': an overview of the experimental conditions that were re-created deterministically by each code. Most coarse mesh CFD codes were only applied to 30 min run 10050401 (first run of test 100504, see Section 2). As explained before, the wave input for OFA1 and OFA was different. The screening results for the 3 h and 30 min durations cannot be directly compared, because especially the 30 min results are probably not converged. This is no problem for deterministic relative comparison, but it is for comparison to another duration. Two groups of results (3 h and 30 min) are therefore discussed separately in the following sections. In order to relate the 30 min results to the 3 h results, the PRE and OFA results were also added to the 30 min comparisons.

Table 2 also provides an overview of the considered green water indicators per tool. The experimental indicators are included for reference. These provide a baseline for some indicators: no matter how well the RWE is calculated, it will probably not serve as a better indicator than the experimentally measured RWE. Possible green water indicators such as crests in undisturbed wave elevation, peaks in RWE at different locations, their rise time and crest front steepness (both defined in Section 4) and troughs in vertical bow position and velocity were calculated. The coarse mesh CFD indicators also include the coarse mesh force over the total breakwater, and on the bottom row of 8 force panels. This force will likely not be calculated accurately, as that would

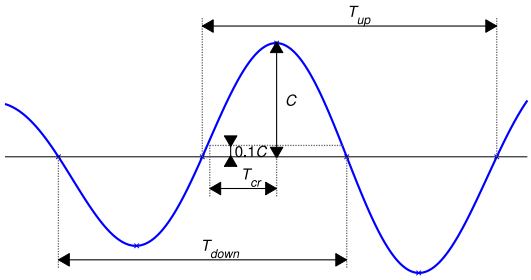

Fig. 8. Wave definitions.

require a much finer mesh (see Bandringa et al., 2020). However, the idea of screening is that the relative order of the impact forces from the coarse mesh calculations is similar to the order of 'real' impact forces from the experiments or fine mesh CFD calculations. This would make it useable for screening. Other coarse mesh indicators are the peaks in the water fluxes through three vertical planes on deck (definition see Appendix A). Signal peaks and their rise time and crest front steepness are defined in Section 4.

4. Definitions

4.1. Failure mode

The target of any screening exercise is the prediction of a failure mode: the critical design load on a structure. In the present study, this is defined as a large total green water force in x-direction on the breakwater of the KCS. In the experiments this was derived from the sample by sample sum of all 40 breakwater panel forces (Fig. 4). Any mention of *FX* in the present publication refers to this total force. It can be discussed whether typical deck structures are most sensitive to the peak force value, or to the duration or total impulse of the green water force. This depends on the specific structure. The peak forces were deemed most critical for the relatively large breakwater structure, so these are used as failure mode in the present study. Some of the screening quality work was repeated for the prediction of impulse of the force peaks. This showed that it is slightly easier to predict force impulse than peak force. This may be because peak forces are more sensitive for small details in the flow, and therefore vary more for the same indicator peak value. This is not further elaborated here.

4.2. Rise time and crest front steepness

The rise time T_{cr} of a peak in a signal is defined as the time between the peak and the last previous time that the indicator reached 10% of the peak value in the time trace (see Fig. 8). The dimensionless crest front steepness ϵ of an indicator peak is defined as in Myrhaug and Kjeldsen (1986), but modified to include the T_{cr} defined here. This is defined in Eq. (1), where C is the crest or peak height and T_{down} the zero down-crossing period around the considered peak. Especially the crest front steepness is sensitive for discontinuities in the signal, which are mainly due to concatenation of the different experimental runs in a 3 h test. Peaks very close to run changes were therefore removed from all time traces before further analysis.

$$\epsilon = \frac{2\pi C}{g T_{down} T_{cr}} \tag{1}$$

4.3. Matching peaks in indicator to peaks in failure mode signal

In order to evaluate the screening quality, it is required to deterministically match peaks in an indicator signal to experimental force peaks. This is not straightforward. There is usually a time difference between an indicator peak and the corresponding impact force peak, and not each indicator peak leads to a force peak. The time difference depends on the type of green water event (hammerfist, plunging, scooping, ...), the selected indicator and its location with respect to the deck structure, the wave propagation velocity and kinematics, the propagation velocity of the green water over the deck and the ship motions. Two different correlation methods to couple indicator peaks $\hat{i}(p)$ to corresponding failure mode load peaks $\hat{f}(p)$ were therefore used, depending on the type of indicator signal (where p is the peak index). In both cases, first all start-up and end effects were removed from the experimental and numerical time traces.

A correlation method based on the indicator zero up-crossing times $t_{zu,i}(p)$ was used for continuous signals such as undisturbed wave elevation, see Eq. (2). The maximum load between each set of indicator zero up-crossings was coupled to the associated zero up-crossing indicator peak. This does not have to be a peak load, simply the maximum measured value from the experiments within this interval was taken. The result of this procedure is illustrated in Fig. 9 on the left.

$$\hat{i}(p) = \max\left[i\left(t_{zu,i}(p) \le t < t_{zu,i}(p+1)\right)\right] \tag{2a}$$

$$\hat{f}(p) = \max\left[f\left(t_{zu,i}(p) \le t < t_{zu,i}(p+1)\right)\right] \quad \text{for continuous signals} \tag{2b}$$

For more 'peaked' indicator signals without zero crossings such as relative wave elevation on deck, an alternative correlation method based on time intervals of a few seconds around peaks above a threshold was used (see Eq. (3)). The intervals based on the indicator peaks usually do not fully cover the time trace, which could lead to missing important force peaks. Therefore a 'two-way' version of this matching method was applied: using both the indicator and failure mode peaks as lead signal. The times of the peak over threshold indicator peaks $\hat{t}_i(p)$ and of the failure mode peaks $\hat{t}_f(p)$ were joined. The threshold for

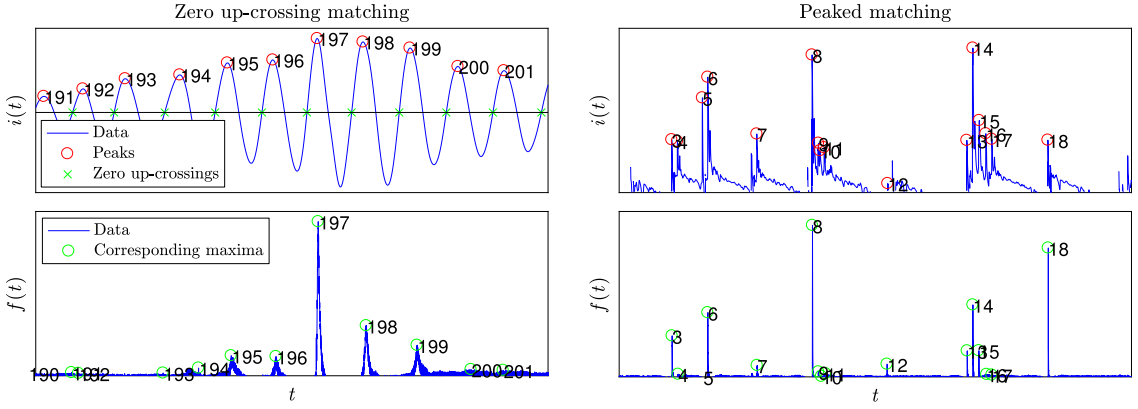

Fig. 9. Zero up-crossing matching method (left) and peaked matching method (right), where $i(t)$ is the indicator time trace and $f(t)$ is the synchronised failure mode time trace. Parts of example time traces.

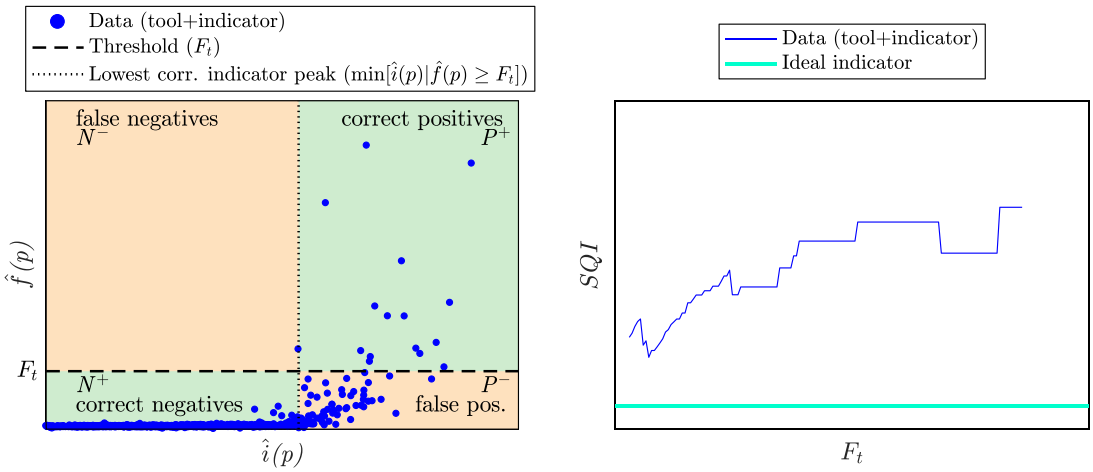

Fig. 10. Scatter plot of failure mode maxima versus indicator peaks for an example indicator (left) and the corresponding screening quality index as a function of failure mode threshold (right).

this peak over threshold analysis is selected just above the noise level of each signal. A time interval of a few seconds d was then applied in order to remove grouped peak intervals. Next, the maximum indicator value and maximum failure mode value were determined for each interval around the joined peak times $\hat{i}(p)$. The result of this procedure is illustrated in Fig. 9 on the right. The same procedures can also be used to link to signals of the same type, for instance to make a scatter diagram of numerical wave crests versus experimental wave crests.

$$\hat{i}(p) = \hat{i}_i(p) \cup \hat{i}_f(p)\Big|_{\text{grouped, 1 peak within d}} \tag{3a}$$

$$\hat{i}(p) = \max\left[i\left(\hat{i}(p) - \mathrm{d} \leq t < \hat{i}(p) + \mathrm{d}\right)\right] \tag{3b}$$

$$\hat{f}(p) = \max\left[f\left(\hat{i}(p) - \mathrm{d} \leq t < \hat{i}(p) + \mathrm{d}\right)\right] \quad \text{for 'peaked' signals} \tag{3c}$$

4.4. Screening quality index

The quality of the identification of critical events by a combination of calculation tool and indicator is expressed by the 'screening quality index' SQI. First, indicator peaks from a numerical tool were matched deterministically to force peaks from the experiments (see Section 4.3). A false negative occurs when the indicator does not predict a green water event, but it nonetheless occurs. A false positive occurs when the indicator predicts a green water event, but the event does not occur. A green water event is defined as a force on the breakwater above a given threshold (see Section 4.1). Forces below this threshold are not considered green water events that need to be captured. SQI is then defined in Eq. (4), and visualised in the left plot of Fig. 10. It is equal to the ratio of total number of positives over the number of correct positives, allowing no false negative above the threshold load (horizontal line in scatter plot). In the formulation, P^+ are all correct positive events, P^- are all false positive events, $\hat{i}(p)$ and $\hat{f}(p)$ are still the matched indicator and force peaks, p is the matched peak index and F_t is the considered force threshold. $\mathrm{n}(X)$ indicates the number of elements in X.

$$SQI(F_t) = \frac{\text{total \# of positives } (F_t)}{\text{\# of correct positives } (F_t)} = \frac{\mathrm{n}\left(P^+(F_t) + P^-(F_t)\right)}{\mathrm{n}\left(P^+(F_t)\right)} = \frac{\mathrm{n}\left(\hat{i}(p) \geq \min\left[\hat{i}(p)|\hat{f}(p) \geq F_t\right]\right)}{\mathrm{n}\left(\hat{f}(p) \geq F_t\right)} \tag{4}$$

The most left data point above the force threshold in the scatter plot of Fig. 10, corresponding to a low indicator peak but a relatively high force peak, determines SQI. A perfect indicator leads to $SQI = 1$ for all thresholds. In that case, every considered indicator peak corresponds to a significant force peak, and the scatter plot shows a linear relation with points only in the correct positive and correct negative areas. The thus defined SQI can be plotted as function of force threshold. Increasing the threshold moves the horizontal line in the left plot of Fig. 10 upwards over the y-axis. The resulting SQI can be found using the same threshold on the x-axis of the right plot. The right plot can be used to compare different tool and indicator combinations. Each combination adds a line to such a plot, and the lowest line corresponds to the best result. As the present publication includes a large number of wave conditions, numerical tools and indicators, the overall comparison will be made based on a reduced dataset.

For this purpose, firstly the SQI corresponding to the 10th-highest force peak was used. This ensures that the 10 highest force peaks in each test are predicted. The number of correct positives is then equal to 10 for each test, regardless of the numerical tool and indicator. This corresponds to a different force threshold per sea state (see Table 3). For reference, the maximum measured force per test is also given. This shows that the maximum force in 30 min run 10050401 is close to that in 3 h test 100504 (a run with a large peak was selected), but the 10-event threshold is lower due to the shorter duration. Assuming that a screening approach as described in Section 1.1 needs high-fidelity calculations for the 10 highest load peaks in step 5, the number of events to run in e.g. fine mesh CFD is equal to 10 times SQI. An ideal indicator would predict all of them correctly ($SQI = 1$), which means that 10 events need to be run. Secondly, the average SQI over the full range of thresholds (up to the maximum experimental force per test) was used. Whether aiming for the 10 highest force peaks in 3 h is a good goal for a screening study needs to be evaluated in a follow-up study. The present study will compare indicators and tools in a relative sense, the outcome of which is not expected to change significantly based on the force threshold. Both the 10-event and average SQI values are used for this purpose.

5. Results and discussion

5.1. Wave and response time traces

The basis for the screening results described in the following sections are the time traces of waves and ship responses from the experiments and numerical tools. These time traces can also be compared directly, which may help to find the cause of good or bad screening performance. An outlier in a screening quality plot can probably be related to the numerical reproduction of the waves, or to the prediction of the ship response. However, direct wave and response comparison is not the main purpose of the present paper. These results are therefore concisely discussed in Appendix B. The main conclusions are summarised here.

Table 3
Experimental *FX* peak threshold for the 10 highest peaks per wave condition, and the maximum measured value per test for reference.

Test no.	100501	100502	100505	100504	100506	100702	100705	100703	100704	(10050401)
Duration [h]	3:16	3:08	3:08	3:14	3:06	3:20	3:14	3:15	3:11	(0:30)
Max. measured *FX* [mN]	40.1	84.6	9.6	14.7	6.1	17.1	16.4	8.6	17.2	(13.7)
10-event *FX* threshold [mN]	27.4	37.4	5.9	4.2	2.3	4.7	3.6	4.7	7.8	(1.2)

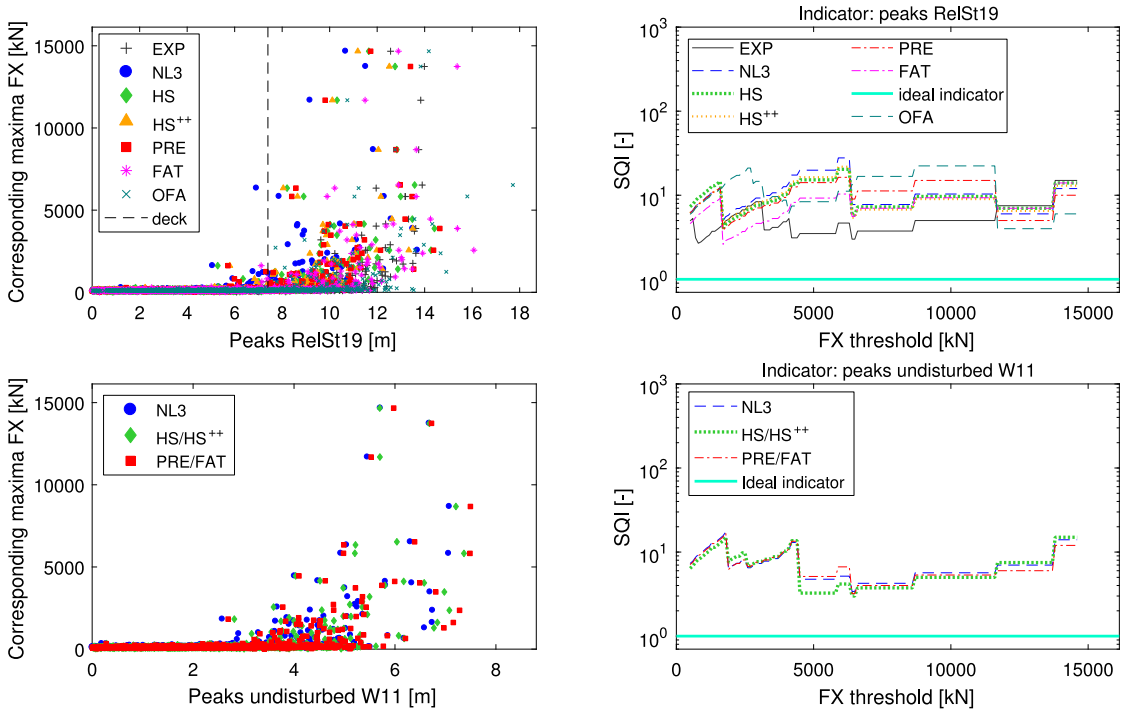

Fig. 11. Scatter and screening quality plots, example test 100504, indicator peaks in RelSt19 (top) and undisturbed wave elevation at W11 (bottom, propagated with linear dispersion from W1).

The considerations in Section 3 lead to some differences in input waves between the different codes. Linear propagation from the wave probes to the COG was used for all potential flow codes, which introduces similar errors compared to the real non-linear properties of the steeper wave conditions (negligence of higher-order wave–wave interactions and wave breaking). The Appendix also shows some differences between the different potential flow wave results. Due to analytical post-processing of the experimental wave measurements (Fig. 6), HS/HS^{++} underpredicts the highest undisturbed wave crests. As the largest green water impacts are probably related to large and steep waves, this could be an issue for screening. This is further discussed in the next sections. The coarse mesh OpenFOAM undisturbed wave results (OFA, available for one 3 h test) deviate more from the experiments than the potential flow results. The Appendix explains that this is probably mostly due to the choices made for the OFA wave input. Linear analytical wave elevation propagation from the experimental measurements at W45 to the inflow location was used and linear wave kinematics were added, after which the waves were propagated in the CFD code to the model and the other probes (see Fig. 7). The coarse mesh CFD wave results for 30 min run 10050401 show how these results could be improved, for instance by defining the inflow directly at an experimental wave probe location, and adding second — instead of first-order wave kinematics. These results also show significant differences in undisturbed waves at W11 (close to the ship bow) between the coarse mesh CFD codes, especially for the higher wave crests. The OFA1 and OFB results are very similar and quite far below the experimental results for the highest wave crests, whereas the highest ComFLOW crests are closer to the experiments, with a slight overestimation of the largest crests. The differences in undisturbed waves between the three ComFLOW grids CF1-3 are small.

The ship response results (heave, pitch, relative wave elevation RWE) from all potential codes and coarse mesh CFD codes are relatively close to the experiments, but they are even closer to each other. There is no significant difference between the time-domain and frequency-domain codes, between the Rankine-source or zero speed Green's function codes or between linear and weakly non-linear codes. The coarse mesh CFD results are also very close to the potential flow results. The considered speeds are probably too low to show much better results with Rankine-source codes, and the motions are relatively small in the steep short waves, so the Froude–Krylov force components are also small. On average, both the heave and pitch motion peaks are overestimated compared to the experiments by all codes, which may be due to the absence/underestimation of small viscous damping effects in potential flow and coarse mesh CFD. The largest RWE peaks were slightly overestimated by all potential flow codes compared to the experiments. This may be due to water flowing over deck in the experiments, wave breaking that lowers experimental RWE for the highest peaks or overestimation of the numerical ship motions. The similarity in heave, pitch and RWE results indicates that the coarse mesh CFD screening results are not expected to be much better than the potential flow screening results. On the other hand, the extra indicators such as wave elevation on deck, forces and fluxes that CFD can produce may be valuable extra indicators. This is discussed in the next sections.

5.2. Screening quality index for 3 h tests

The screening quality was evaluated for all considered codes, indicators and 3 h tests. The results of the potential flow codes were provided based on linear wave propagation from the 'best probe' discussed in Section 3.1. The results from coarse mesh CFD code OFA are also

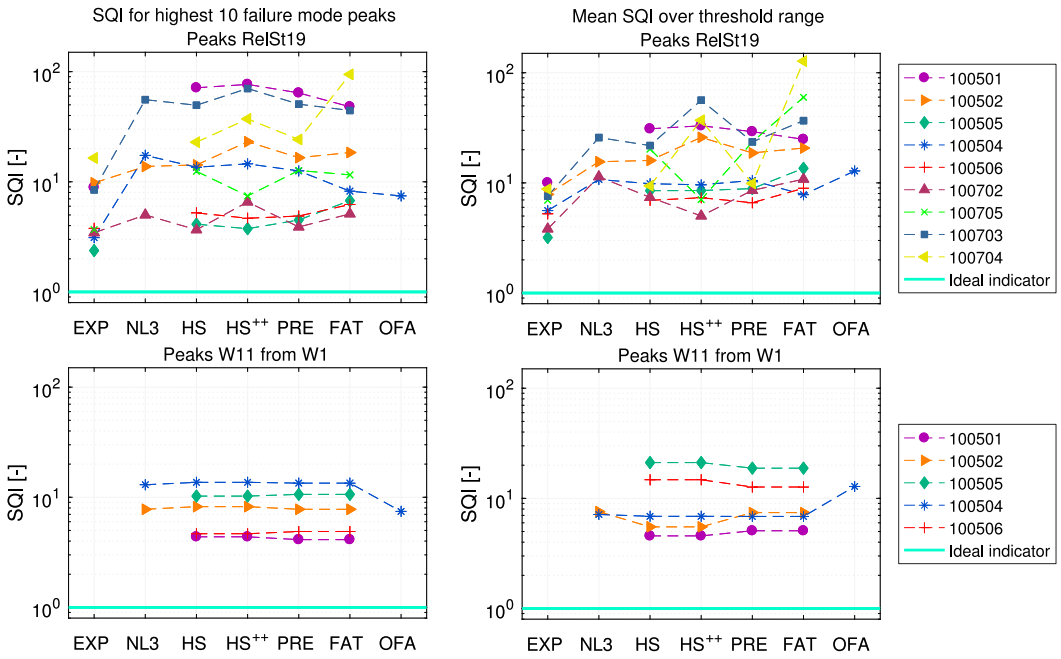

Fig. 12. Screening quality for 10 highest peaks (left) and average over threshold range (right) per 3 h test, indicator peaks in RelSt19 (top) and undisturbed wave elevation at W11 (bottom, propagated with linear dispersion from W1).

included for one of the 3 h tests. The screening performance of the other coarse mesh codes (based on the 30 min run) are discussed in Section 5.3. Not all codes were run for all tests and indicators (Table 2). For consistency, the legends of the plots in the present section contain all codes, but the missing entries are empty. The plots also include the results for experimentally measured indicators where possible.

The indicator peaks were matched to the experimental force peaks using the matching procedure in Section 4.3, after which the SQI was derived according to Section 4.4. For each of the available indicators and each of the nine 3 h tests, a scatter plot of indicator versus force peaks and a SQI plot as function of force threshold was thus generated. Such plots are shown in Fig. 11 for one example test (100504) and two example indicators (peaks in RelSt19 and crests in undisturbed waves at W11). The second indicator was not directly delivered by the potential flow codes, it was derived by wave propagation according to linear dispersion from the time traces delivered at probe W1, as explained in Section 3.1. This indicator was not calculated with OFA. Scatter plots for the other indicators for the same example test, and for the two selected indicators for all other 3 h tests are shown in Appendix C. All other scatter plots are omitted from the present publication, but their summary values are included in the further discussions. These plots show that some of the considered indicators are quite bad, such as the troughs in vertical bow motion or velocity, or the inverse of the rise time of RWE at the bow. Their relation with the experimental force peaks is far from linear. Other indicators perform better. The two selected indicators in Fig. 11 are two of the best performing indicators, with numerical SQI values between 3–20 over the full threshold range. This will be confirmed in a comparison of all indicators in Section 5.5.

As explained earlier, SQI is quite sensitive for outliers. Appendix D highlights four events, showing the calculated indicator peak, the corresponding experimental force peak, its position in the scatter and SQI plots and some video snapshots. Summarising, some events are associated with relatively low but steep waves, with high horizontal water velocities in the crest. If these crests just exceed the freeboard, they may be translated to a relatively low RWE but a high-speed jet over the foredeck that impacts the breakwater. These events are not well captured when the peaks in RWE at the bow are used as indicator (but may be by for instance peaks in non-linear horizontal water velocities in the wave crest). Secondly, there are the higher steep wave crests breaking over the deck. The linear RWE serve reasonably well as indicator in these cases, but including some higher-order incoming wave components associated with high breaking wave crests could improve the results. It seems logical that the water sometimes comes from another side than where the relative wave probe is located, which would lead to a bad screening performance for that event. However, no big SQI-determining outliers due to this principle were identified in the RWE results. Missing non-linearity in the RWE peaks and missing (non-linearity in the) water velocities in the wave crests seem the determining factors for the force peaks that are not well predicted.

The SQI for prediction of the 10 highest events and the mean SQI over the threshold range (both described in Section 4.4) were derived from these plots for all tests and indicators. These plots are presented in Fig. 12 for the same two example indicators. These figures show quite some variation between the different tests, but some general trends can be identified. Most potential flow codes perform very similarly in head waves (test numbers 1005xx). For the bow-quartering waves (1007xx) there is more variation, but not always towards higher SQI and worse screening performance. For the two tests at a higher speed of 10 kn (100502 and 100704), it was expected that Rankine-source codes NL3 and FAT would perform better than the other codes. However, this is not clearly visible in the results. This may be because this speed is still limited. For higher speeds these codes may perform better in a relative sense, but that is not very realistic for a containership in severe wave conditions. The weakly non-linear motion codes NL3 and HS^{++} also perform similar to the linear codes. This is probably because the ship motions were small in the given steep wave conditions. The steepness of the waves itself does seem to play a role in the screening performance. As expected from potential flow, a better performance was found for the least steep wave conditions such as test 100505, 100506 and 100702. However, this effect is not very strong, and mixed with speed, wave height and heading effects. As it is complicated to obtain an overview of these results, they are averaged over all tests or different groups of tests in Section 5.5 (after a similar analysis of the 30 min run in the next section).

5.3. Screening quality index for 30 min run

For the 30 min run 10050401, similar scatters of indicator peaks versus experimental force peaks were made, and the corresponding

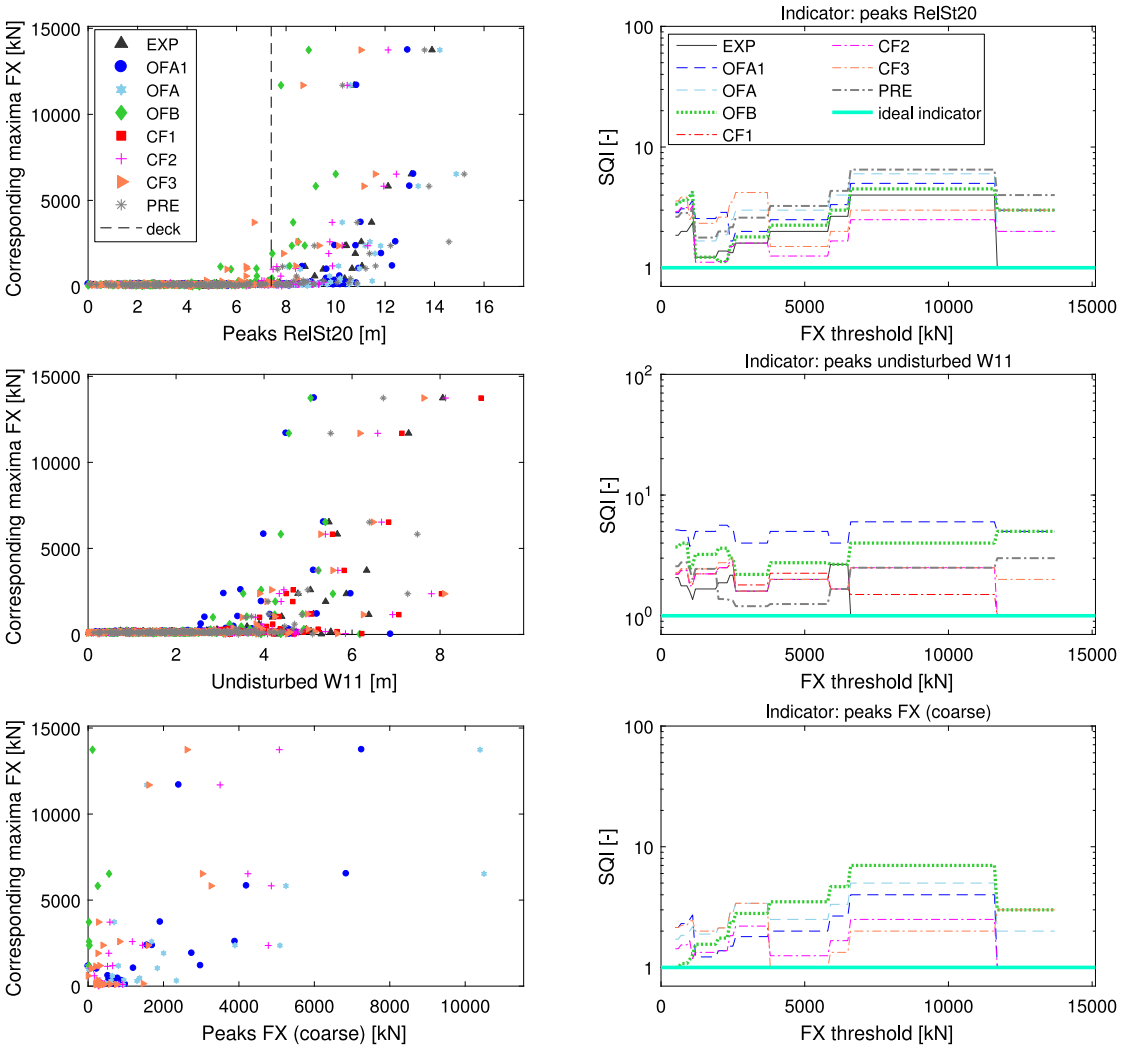

Fig. 13. Scatter and screening quality plots, 30 min run 10050401, indicator peaks in RelSt20 (top), crests in undisturbed wave elevation at W11 (middle, where PRE = linearly propagated from W1) and coarse mesh total force on breakwater (bottom).

SQI plots over the full threshold range. The results are shown in Fig. 13 for example indicators peaks in RWE at RelSt20, crests in undisturbed waves at W11 and peaks in coarse mesh total force on the breakwater. Similar plots for the other indicators in Table 2 are omitted here. The peaks at relative wave probe RelSt20 were selected here as example instead of the results at RelSt19 (which served as example indicator for the 3 h tests), because only a few of the coarse mesh CFD codes delivered results at RelSt19. At a first glance, the scatter plots for the 30 min coarse mesh CFD results look similar in number of outliers and amount of scatter as observed for the 3 h potential flow results. This is confirmed by the potential flow result PRE that is included in these 30 min plots. The coarse mesh CFD codes lead to lower SQI values, but only marginally. The overview of the SQI for the 10 highest peaks and the mean over the threshold ranges are directly presented in the 'final overview' Section 5.5. This section also includes a discussion of the difference between the coarse mesh CFD codes.

5.4. 3 h versus 30 min results

As explained in the introduction, a converged very long duration result is not required for the present deterministic comparison to the test results. This means that the SQI values are not converged (especially not in 30 min), so the different durations cannot be compared one to one. Fig. 14 shows the difference between the 3 h test 100504 and its first run 10050401. This shows indeed that the values based on the single run are lower. However, the relative order between the results from the three different tools is largely the same for the long duration test and the single run (as expected). This means that we can use the comparison to help determine which tools are expected to show the best green water indicators.

5.5. Final overview of screening capabilities and computational times

The present section compares the screening quality results for all indicators and tools and both test durations. If only the quality would be assessed, fine mesh CFD tools and experiments would 'win' the competition. However, we know that it is (presently) not feasible to screen a full scatter diagram with such tools. The required computational times of the different tools are therefore also evaluated: the higher the screening quality and the faster the tool, the more suitable it is for screening. The SQI for the 10 highest events and the average SQI over the threshold range from all 3 h tests are shown in Fig. 15. This plot includes all indicators and tools discussed in Section 5.2 that are available for at least four of the 3 h tests, and it shows average results over all tests or groups of tests. A similar plot for 3 h test 100504 only is shown in Fig. 16, also including coarse mesh CFD code OFA. Finally, Fig. 17 shows similar results for the 30 min run 10050401, based on the results in Section 5.3. The computational times that were required in order to obtain these results are listed in Table 4 (3 h tests) and Table 5 (30 min run), where CPUh is defined as wall

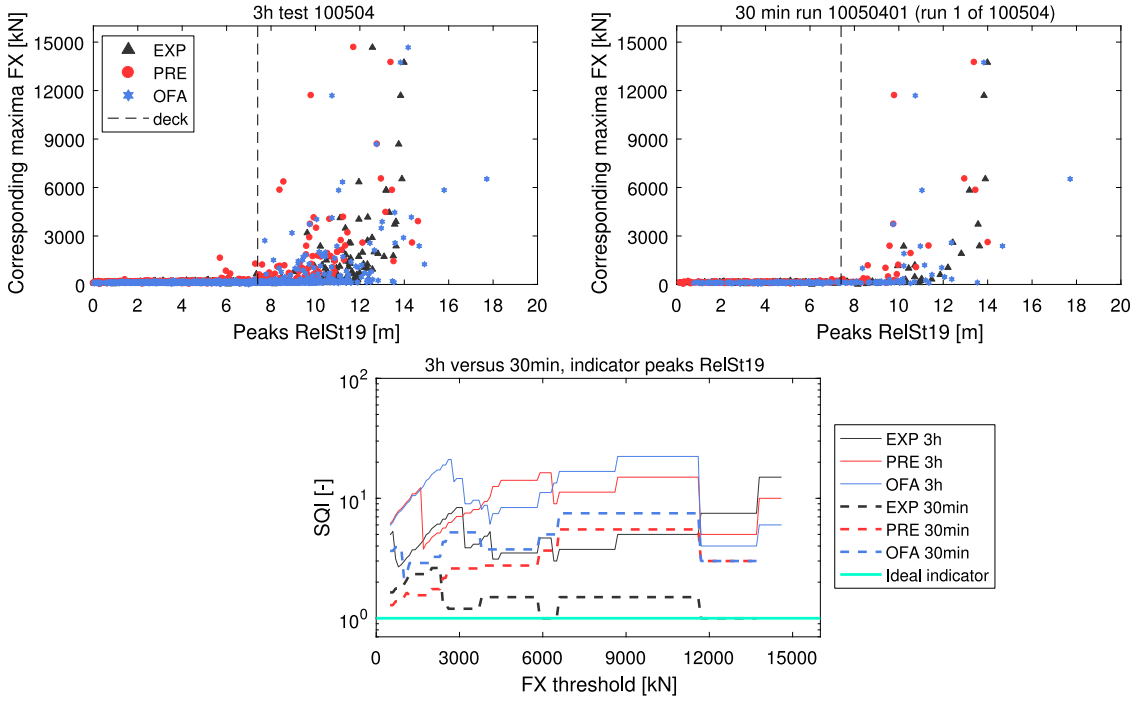

Fig. 14. Peaks in RelSt19 scatter and screening quality plot for 3 h test and first 30 min run from this test, indicators that are available for both.

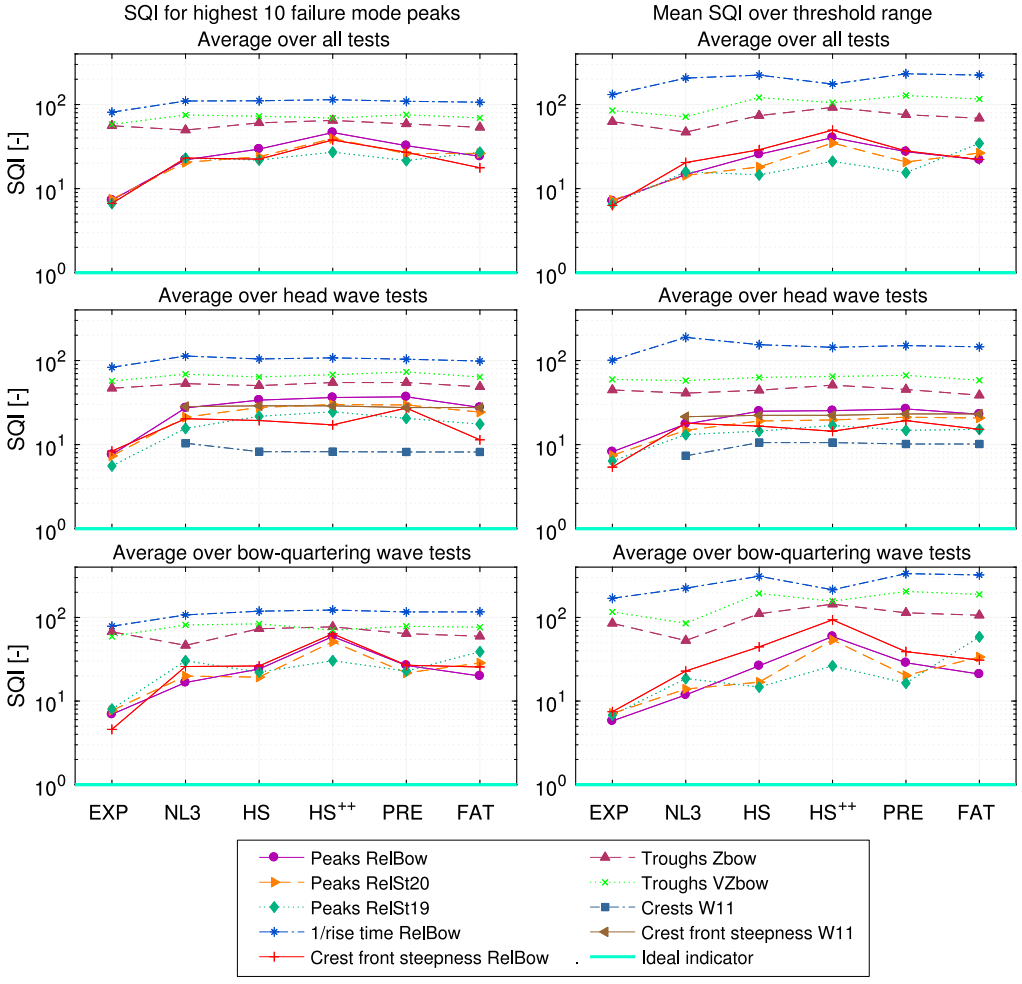

Fig. 15. Potential flow and experimental screening quality for all indicators in all 3 h tests for the 10 highest peaks (left) and average over threshold range (right), mean over all tests or over tests in head or bow-quartering waves.

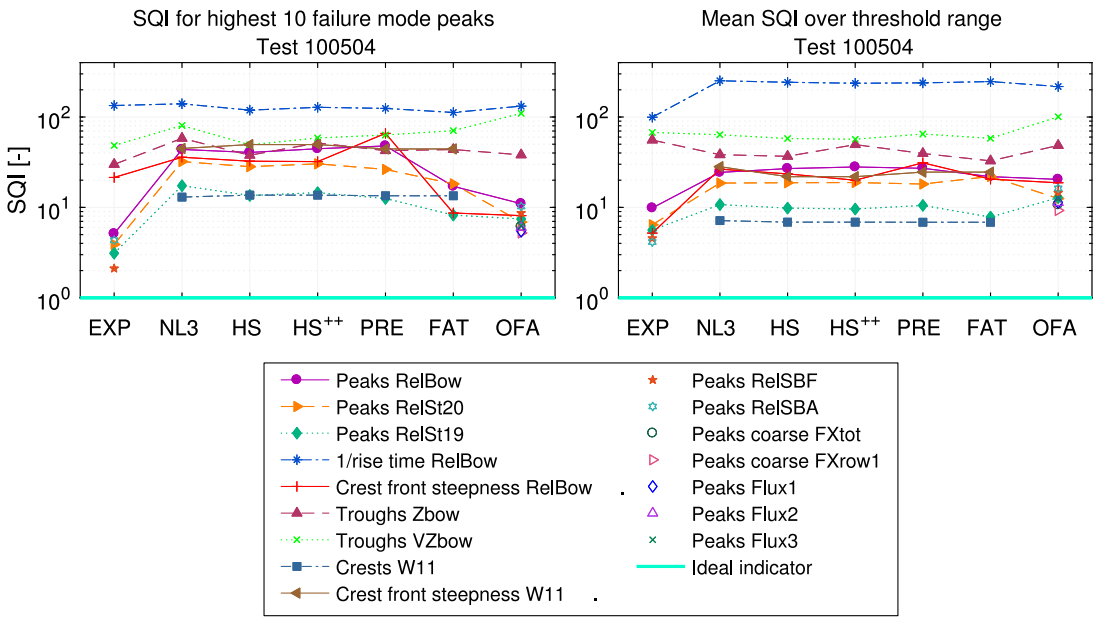

Fig. 16. Potential flow, coarse mesh CFD and experimental screening quality for all indicators in 3 h test 100504 for the 10 highest peaks (left) and average over threshold range (right).

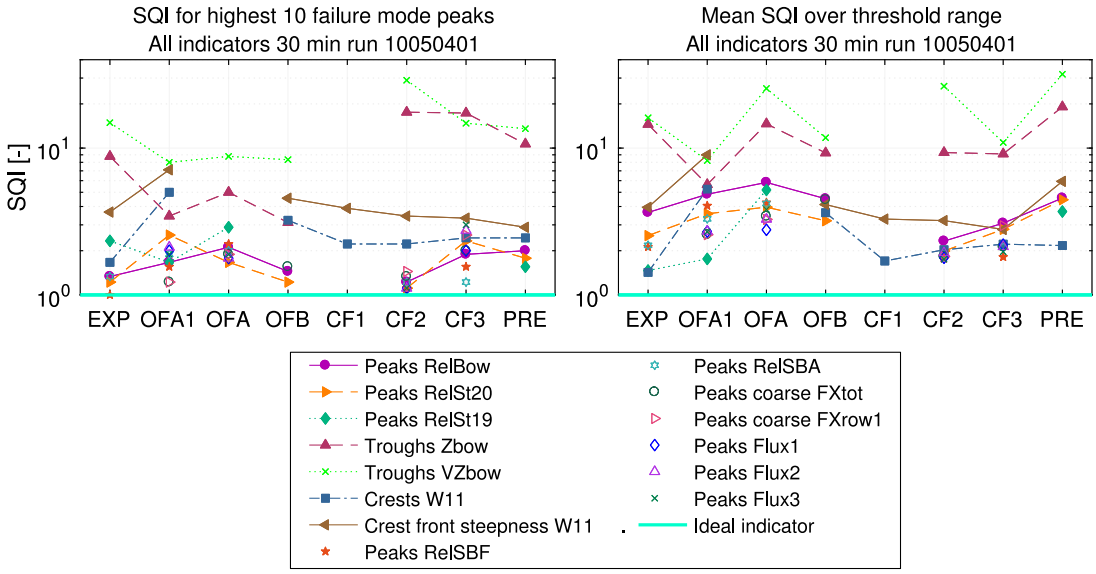

Fig. 17. Coarse mesh CFD, PRE and experimental screening quality for the 10 highest peaks (left) and average over threshold range (right) for several indicators, 30 min run 10050401 only.

clock time times the number of cores on which the calculation was run. The computational times for the frequency- and time-domain tools scale differently: frequency-domain codes are relatively expensive for short durations, but cheap for a large number of conditions. All coarse mesh CFD computational times were much longer than the potential flow times, as expected. Still, these times are significantly reduced compared to what would be required for a fine mesh simulation of the same duration. OFA1 required a longer computational time for the 2D waves than OFB, whereas this is the other way around for the 3D simulation. This has to do with the adaptive time stepping used in the 3D simulation in OFB (Appendix A). The required computational times for the ComFLOW calculations are significantly shorter than for the OpenFOAM simulations, especially for the coarsest grid. This probably has to do both with the Cartesian grid modelling and the choices for the time steps and grid cells.

As expected, Figs. 15 to 17 show that the experimental indicators perform better than those from the numerical tools for almost all measured indicators. The differences in performance between the different potential flow codes are very small, especially in head waves. This is good news; it does not matter a lot which potential flow code is available. As discussed in Section 5.2, the codes with zero speed Green's function or Rankine-source diffraction, linear or weakly non-linear Froude–Krylov, frequency- or time-domain perform very similarly. In bow-quartering waves, only HS^{++} and FAT perform slightly less good than the other codes, and NL3 slightly better. This is not due to the wave input in HS^{++} or FAT, as that is the same as in respectively HS and PRE.

Over all 3 h tests, the indicators peaks in RelSt19, RelSt20 and RelBow perform quite well, as well as the crest front steepness of RelBow. In head waves, the undisturbed wave elevation at W11 performs even better. This indicator was not evaluated in bow-quartering waves, but

Table 4
Computational times required to obtain the 3 h numerical results in CPUh (defined as wall clock time times number of cores, so for example 1× 3 h OFA simulation takes 35 980/96 ≈ 375 wall clock hours), all 3D simulations with ship.

Code	NL3	HS	HS^{++}	PRE	FAT	OFA
# cores used	1	4	4	12	2	96
# CPUh for database frequency domain	–	1	–	2	27	–
# CPUh for 1× 3 h simulation	5	1	0.3	2	27	35 980
# CPUh for 9× 3 h simulation	43	1	3	2	27	~323 820 (extrapolation)

Table 5
Computational times required to obtain the 30 min numerical results in CPUh (defined as in Table 4).

Code	OFA1	OFA	OFB	CF1	CF2	CF3	PRE
# cores used for 2D	16	–	4	8	1	1	4
# cores used for 3D	96	96	96	–	8	8	4
# CPUh for database frequency domain	–	–	–	–	–	–	2
# CPUh for 1× 30 min 2D simulation waves	19	–	9	13	3	1	2
# CPUh for 1× 30 min 3D simulation with ship	4401	4986	28 896	–	416	56	2

there is no reason to assume that it will work significantly less good for this heading. This may open the road for the use of non-linear wave modelling tools without ship for screening (e.g. non-linear potential flow, coarse mesh volume-of-fluid or particle methods), although the effect of forward speed would need to be considered.

Based on the 3 h results for test 100504 (Fig. 16), it can be observed that coarse mesh CFD code OFA and the potential flow codes lead to similar screening quality results for the indicators that were calculated with both, such as crests and crest front steepness of RWE and of undisturbed incoming waves. The additional OFA indicators related to peaks in coarse mesh breakwater force, RWE on deck and fluxes through planes on deck also lead to similar or slightly better SQI values. The wave input in the long duration OFA calculations could be improved, but this is also valid to some extent for the potential flow results. Comparing OFA with the other coarse mesh CFD tools in the 30 min run will show how much improvement could be expected. However, Table 4 shows that the required computational time to reach these similar results for one 3 h simulation is a factor 1000–100000 (depending on reference code) higher than that for the potential flow codes.

As said, the SQI for 30 min cannot be directly compared to the SQI for 3 h, but the relative ordering of the different codes is assumed to be comparable. Similar to the 3 h results, the 30 min results in Fig. 17 show that good results were achieved with peaks in RWE around the bow as indicator, with the lowest value for the experimental measurements (as expected). All coarse mesh CFD codes and PRE also lead to low values for this indicator. The crests in undisturbed wave elevation at W11 also perform well, especially based on the average SQI over the threshold range. The PRE result in that case is the propagated wave elevation using linear dispersion from the W1 measurements including ship model. The CFD-specific indicators peaks in RWE on deck, peaks in coarse mesh breakwater force and fluxes through planes on the fore deck also perform well, in some cases even slightly better than the peaks in RWE.

OFB and OFA (run 1 of the 3 h test 100504) perform least well compared to OFA1 and the CF1-3 results. The difference between OFB and OFA1 is mainly due to grid and time step settings (Appendix A). The choices made in OFA1 seem better suited to screening, leading to lower SQI values against much shorter computational times (Table 5). The difference between OFA and OFA1 is only the wave input; as expected the OFA1 undisturbed wave input leads to better results. In CF1-3, a lot of attention was paid to the quality of the wave. Appendix B shows that the ComFLOW undisturbed waves match the experiments better than the waves in all versions of OpenFOAM. Fig. 17 shows that this also translates to lower SQI values, especially for grid 2 (CF2). As the wave input methods were different as well as the applied code and grids, the main cause for the differences cannot be identified. However, it is likely that the wave input and the grid and time step settings play a large role. This implies that the OFA results in the 3 h test 100504 presented in Fig. 15 could be improved by improving the wave input method and possibly the grid and time step settings. CF2 or CF3 seem the most suitable combinations of tool, wave input, grid and time step settings for coarse mesh CFD screening. They lead to the lowest SQI values of all coarse mesh CFD codes (Fig. 17), against the shortest computational times (Table 5). CF2 is slightly slower but with better SQI results, CF3 is faster but with slightly less good SQI results. Still, these coarse mesh CFD tools deliver only marginally better or even similar SQI results to the reference potential flow code PRE, while they take 416 or 56 CPUh, against 2 CPUh for the full PRE database. This is a factor 20–200 in computational time increase for a factor 1–2 SQI improvement.

5.6. High-fidelity force distribution based on screened events

As explained above, potential flow methods are quicker than coarse mesh CFD and a have similar or only slightly lower screening quality. As explained in Section 1, it may also be possible to apply RCM based on the linear response functions from potential flow to further speed up the screening. However, in order to run the selected linear wave events in CFD without missing important higher-order wave effects, a method such as the Event Matching in Johannessen and Lande (2018) is required (but then with ship motions and forward speed). A possible motivation for eventually selecting coarse mesh CFD for screening can be found when considering the next step in the green water analysis, where events identified by the screening method need to be assessed in detail using a high-fidelity method. When CFD is chosen for both the screening and the detailed analysis, an automated coupling between the coarse and the fine mesh CFD simulations can be established. This simplifies the workflow significantly. Such a coupling, currently implemented in one of the CFD tools (ComFLOW), allows the events that are identified as critical by the coarse mesh CFD simulation to be re-run automatically on a much finer mesh, to determine the detailed green water loads (as in Bandringa et al., 2020).

This coupling was used to illustrate the feasibility of the screening approach. CF2 was used as screening tool to identify the 10 largest RelBow indicator peaks in the 30 min run. Fig. 17 shows that CF2 indicator peaks in RelBow has a SQI of 1.2 for the 10 largest events in this run, which is almost perfect. It means that the 12 highest indicator peaks would have to be assessed in order to obtain the 10 highest forces. In a practical problem, the SQI would not be known. Sticking to the 10 highest impact peaks procedure, a fine-mesh ComFLOW calculation was done for each of the 10 highest indicator peaks, using the coarse mesh calculation wave input and ship motions and the fine mesh described in Bandringa et al. (2020). The forces from these 10 fine mesh calculations in combination with the statistics from the coarse mesh calculation lead to the force distribution in Fig. 18. This plot

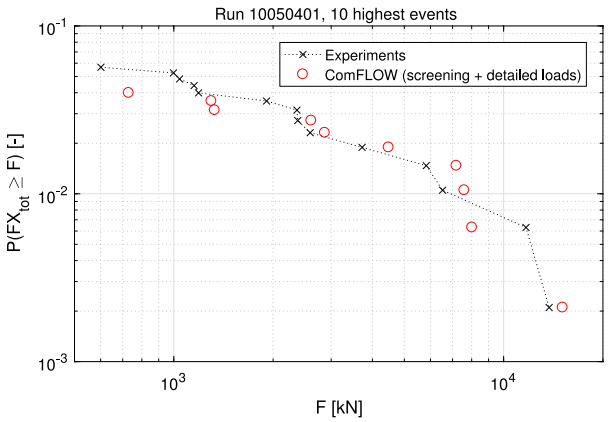

Fig. 18. Distribution of total green water force on the breakwater in 30 min run 10050401, from experiments and screening procedure. Screening with coarse mesh ComFLOW (CF2, indicator peaks in RWE at RelBow), detailed load calculation for the 10 selected events with fine mesh ComFLOW.

also shows the experimental force distribution for the same run. The probability is given with respect to the number of wave encounters, in this case 238 in the 30 min run. The probability level does not start at one on the top, because most wave encounters did not lead to a green water impact. The figure shows that the distributions are very similar. A Weibull distribution fit to both sets of discrete data points would also lead to similar results. This demonstration shows that the screening procedure is feasible, and leads to the desired results. The screening was not perfect: the order of the 10 highest indicator peaks was slightly different than the order of the 10 highest force peaks. Two of the largest 10 impacts are missing, and two other impacts are included. However, it turns out that these two other events also lead to large loads in this case.

This multi-fidelity screening approach is much quicker than performing the full 30 min run on a fine mesh in CFD, which would be a very heavy computation. It could be further sped up by using a potential flow tool for screening. However, as said that requires some thinking about the use of linear wave input and ship motions as input for the fine mesh CFD calculation. In the overall computational time, screening quality (i.e. the number of events from the screening procedure, with the associated heavy fine mesh computation for each of them) also has to be balanced against the computational time for the screening itself.

In a practical design problem, the approach would not be applied to 30 min of wave data. MCS with the screening tool would be applied, for many wave realisations over a full scatter diagram. RCM could maybe be used to speed up as explained in Section 1.2, but only for screening based on linear Gaussian wave input. A similar plot as Fig. 18 would be made around the desired probability level, where the screening simulation duration determines the probability level that can be resolved.

5.7. Benefit of screening approach compared to common practice

In order to show the benefit of the screening procedure, a brief comparison was made to the contour-line approach discussed in Section 1.2. This method would be used to select a few representative wave conditions from a scatter diagram. As a containership sails around the world, the scatter diagram could be derived from hindcast wave data based on the ship voyages instead of a fixed location. Each of the selected wave conditions would be run in a wave basin experiment, for a large number of 3 h realisations.

Now we consider screening for 3 h example test 100504 with two of the better potential flow indicators: peaks in RWE at RelSt19 from PRE and linearly propagated undisturbed wave crests measured at probe W2 to probe W11. Table 1 shows that 1528 wave encounters were measured in the test duration. Without screening, all of these crests would have to be run in a high-fidelity tool in order to capture the 10 highest green water loads. With screening, this number can be significantly reduced. The left plot in Fig. 12 shows that the 10-event SQI values for these two indicators are 12.6 respectively 13.4. We need to multiply these values with the number of relevant force peaks (10 in this case) in order to determine how many events need to be assessed in a high-fidelity tool. This leads to 126 respectively 134 events, which is a reduction of 91%–92% compared to all wave encounters. In the present experimental dataset only one 3 h realisation is available per wave condition, whereas a number of realisations of this duration would be run in the contour-line approach. If the screening target would be to identify the 10 highest events in each realisation, the ratio of events to analyse with and without screening will be the same for more realisations (so still 91%–92% reduction). If the target is to identify the 10 highest events over all realisations, the ratio will probably be even more favourable for screening. Assuming that the 3 h SQI is converged and assuming that 20 realisations of 3 h duration would be required, this could reduce the number of events with even ~99.6% (1–130/(1528*20)). The computational time with screening tool PRE in order to achieve this is only 2 CPUh (see Table 4). This could possibly be further reduced using RCM, although generating the frequency-domain database is more 'expensive' than running the MCS for 20 wave realisations of 3 h. This may translate to a significantly shorter experimental basin time or lower number of fine mesh CFD calculations.

These percentages are rough indications, that do not consider the required 'pre-event' time in a high-fidelity analysis or the groupiness of events. It is not possible to run only one wave crest in a high-fidelity tool, which reduces the efficiency of the screening compared to the numbers above. On the other hand, individual high wave crests usually occur in groups, so a few critical events could probably be grouped in one high-fidelity experiment/calculation. This may partly compensate the pre-event time effect. Finally, the SQI value varies quite a lot with test condition (see Fig. 12), so the reduction will not be as large in every wave condition. However, example test 100504 is not the test with the best result (for these two example indicators the SQI values vary between 4.1 and 64.1 over all nine 3 h tests). The average values in Fig. 15 provide estimates for an arbitrary wave condition.

Summarising, this study shows that a reduction in the order of 90% of the high-fidelity experimental or computational time required to obtain the short-term largest green water loads on a sailing ship can be achieved using a smart screening procedure. However, the amount of saved time depends on the selected indicator and screening tool, on the wave condition and on the balance between groupiness of the indicator peaks and the required pre-event time in the high-fidelity tool.

6. Conclusions

1. Screening for green water events on the breakwater of a sailing containership is feasible. This can be done both with potential flow and coarse mesh CFD codes, provided the indicator is well chosen, as well as the grid, time step and wave input settings.
2. Using linear potential flow means that the input waves are linearised, disregarding the effects of higher-order wave–wave interactions and wave breaking on the identification of the critical events. However, the present study shows that the screening results from linear potential flow are nearly as good as from coarse mesh CFD for the considered test case.
3. The potential flow methods are much faster than coarse mesh CFD, which is favourable for long-term screening. It may even be possible to further speed up the potential flow screening using response-conditioning, as it is based on linear Gaussian wave input (this is not possible for CFD).

4. If potential flow screening is indeed used, questions regarding the use of the low-fidelity screening output in high-fidelity CFD or experiments have to be solved. This is easier for the combination of coarse mesh CFD screening and fine mesh CFD high-fidelity calculations; in that case the required output can directly be generated.
5. The final choice has to be made based on the overall computational time, balancing the time for the screening and the time for the high-fidelity assessment (lower screening quality increases the number of events to evaluate in detail). The low- to high-fidelity coupling may also play a role. Based on the present results, screening with potential flow codes seems the best choice, especially for long-term screening of full scatter diagrams.
6. The peaks in relative wave elevation (RWE) around the bow perform well as green water indicator, as well as the crest front steepness of the RWE. The undisturbed wave crest heights at the bow also seem a good indicator. CFD-specific indicators such as peaks in RWE on deck, in coarse mesh breakwater force and in fluxes through planes on the fore deck perform even slightly better. Missing non-linearity in the RWE peaks and missing non-linearity in the water velocities in the wave crests seem the determining factors for the force peaks that are not well predicted.
7. It does not matter a lot which type of potential flow code is used (zero speed Green's functions or Rankine-source, frequency- or time-domain, linear or weakly non-linear Froude–Krylov modelling). The evaluated potential flow codes NLoad3D, Hydrostar, Hydrostar^{++}, PRECAL_R and FATIMA deliver similar results.
8. The coarse mesh CFD results depend heavily on the choice of wave input, grid and time step settings. Two versions of OpenFOAM and ComFLOW on three grids were compared. The ComFLOW results with grids 2 or 3 seem to be good optima of these choices, leading to quite short computational times and good quality screening results. Still, this is around 2–20 times as computationally expensive as potential flow calculations, gaining only a factor 1–2 in screening quality index SQI.
9. The identified critical wave events based on coarse mesh ComFLOW indicator RWE at the bow were run with fine mesh CFD. This pilot study showed that the resulting load distribution is very similar to the experiments, which shows that multi-fidelity screening is promising for the handling of statistics of extreme events in waves.
10. A smart screening procedure can reduce the required high-fidelity experimental/computational time to obtain the short-term design green water loads on a sailing ship up to 90% compared to full Monte-Carlo simulation. However, the efficiency depends on the selected indicator and screening tool, on the wave condition and on the balance between groupiness of the indicator peaks and the required pre-event time in the high-fidelity tool.

7. Future work

Including some non-linearity in the undisturbed wave or its component in the RWE may further improve the results. This can be done using coarse mesh CFD, but this is computationally expensive. A possibly quicker method could be to use analytical second-order waves or a fully non-linear potential flow method. Both will be evaluated in follow-up project CRS SCREAM (SCReening for Extremes And Maxima in waves). Also, the SQI defined in the present study is a good measure to compare different screening tools in a deterministic validation set-up. However, it also has a few downsides: it is sensitive to outliers, it is not easy to translate to a practical design study and validation requires deterministic reproduction of the wave conditions (Appendix B shows that this is challenging and may lead to worse results than in a 'real' screening application). A statistical approach is therefore foreseen for definition of 'SQI 2.0' that can be used in a design procedure. The idea would be to predict the shape of the load distribution based on a few identified events and the underlying distribution of the indicator. Validation would be based on long duration experiments. This eliminates the need to deterministically reproduce the waves in the numerical tools, and it provides converged statistics for the 1 h or 3 h green water design load. This work will also be part of CRS SCREAM, based on ~20–30 h duration tests with a sailing ferry.

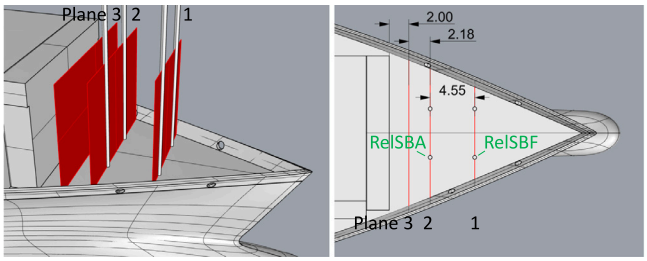

Fig. 19. Definitions of vertical planes on deck through which fluxes in the direction of the breakwater were calculated (plane 1 coincides in x-location with probes PSF and SBF, plane 2 with probes PSA and SBA, and plane 3 is 2 m in front of the breakwater).

Other possible future work could be to combine different indicators to improve the screening performance, or to use large wave groups as indicator (as suggested by Ersdal and Kvitrud, 2000). Applying RCM could further speed up linear screening. Finally, the present validation was based on one ship design in long-crested waves. Variations in wave directional spreading, ship type, bow flare angle, deck layout etc. would increase confidence in the results. In theory, similar screening-based approaches could also be used to evaluate other rare events in waves, such as bow-flare slamming, airgap or wetdeck slamming problems, or even propeller ventilation or parametric roll of ships, overtopping of dykes etc. This requires further study and validation, for which the present publication may serve as a first step.

CRediT authorship contribution statement

Sanne M. van Essen: Conceptualization, Methodology, Writing - original draft, Investigation, Formal analysis, Validation, Visualization. **Charles Monroy:** Conceptualization, Methodology, Investigation, Writing - review & editing. **Zhirong Shen:** Investigation. **Joop Helder:** Conceptualization, Investigation, Writing - review & editing. **Dae-Hyun Kim:** Investigation, Writing - review & editing. **Sopheak Seng:** Investigation. **Zhongfu Ge:** Supervision.

Declaration of competing interest

The authors declare that they have no known competing financial interests or personal relationships that could have appeared to influence the work reported in this paper.

Acknowledgements

The present study was performed within the Cooperative Research Ships (CRS) project Green Water. The authors would like to thank all CRS members for their contributions to this project, and for their commitment to the follow-up project SCREAM. More information: https://www.crships.org/.

Table 6
Relevant properties and settings of applied potential flow codes for screening task 3.3.2 (where ZSGF = Zero speed Green's functions, FK = Froude–Krylov forces, NL = non-linear and FS = free surface).

Name	PRE	FAT	HS	HS^{++}	NL3
Code	PRECAL_R	FATIMA	Hydrostar	Hydrostar^{++}	NLoad3D
Version	18.1.0	2.7	8	8	2.1
Domain	Frequency	Frequency	Frequency	Time	Time
Principle	ZSGF	Rankine sources	ZSGF	ZSGF + FK	Rankine sources + FK
Incoming waves	Linear	Linear	Linear	Linear	Linear
Radiated & diff. waves	Linear	Linear	Linear	Linear	Linear
Motions	Linear	Linear	Linear	Weakly NL	Weakly NL
Full/half hull	Half	Full	Half	Full	Half
# panels (FS+hull)	2038	42 098	1100	18 000	1590
# speeds	2	2	2	2	2
# headings	3	3	3	3	3
# frequencies	73	38	2000	2000	600

Table 7
Relevant properties and settings of applied CFD codes on a coarse mesh (no turbulence models applied). All CFD methods applied to waves with μ 180 deg, H_s 6.8 m, T_p 9.7 s, λ ~147 m.

Name	OFA1	OFA	OFB	CF1	CF2	CF3
Code	OpenFOAM	OpenFOAM	OpenFOAM	ComFLOW		
Version 2D waves	Custom.v4.1	–	v5.x	v4.3.2		
Version 3D with ship	Custom.v1812	Custom.v1812	v5.x	v4.3.2		
Libraries	waves2foam	waves2foam	foamStar120617e	-		
Type of code	Unstructured	Unstructured	Unstructured	Structured (Cartesian)		
Interface reconstr.	No	No	No	Sharp		
Phases	2	2	2	1		
Half/full ship	Full	Full	Half	Half		
CFD scale	Model-scale	Model-scale	Full-scale	Full-scale		
Wave inflow from FPP	172.5 m	172.5 m	134.5 m	At probe W1 (123.7 m)		
Forward speed (kn)	Constant: 5	Constant: 5	Constant: 5	Average: 5		
Fixed motions (zero)	Surge, sway, roll, yaw	Surge, sway, roll, yaw	Surge, sway, roll, yaw	Sway, roll, yaw		
Free motions	Heave, pitch	Heave, pitch	Heave, pitch	Surge, heave, pitch		
Spring	–	–	–	Surge 6.5e6 N/m		
Domain origin	FPP,CL,WL	FPP,CL,WL	St10,CL,WL	W1,CL,WL	W1,CL,WL	W1,CL,WL
Domain x (m)	(−172,680)	(−172,680)	(−596,365)	(0,1200)	(0,1200)	(0,1200)
Domain y (m)	(−284,284)	(−284,284)	(0,347)	(−96,0)	(−96,0)	(−96,0)
Domain z (m)	(−220,110)	(−220,110)	(−190,100)	(−190,35)	(−190,35)	(−190,35)
Far-field grid dx,dy,dz (m)	2.45,9.8,1.13	2.45,9.8,1.13	3.33,13.3,0.83	16,16,16	16,16,16	16,16,16
Near-field grid dx,dy,dz (m)	0.17,?,?	0.17,?,?	0.84,?,0.74	0.5,0.5,0.5	1.0,1.0,1.0	2.0,2.0,2.0
2D wave only						
# cells total	13.6k	–	19k	82k	29k	10k
Time step settings	Constant	–	Constant	Adaptive CFLmax < 0.9	Adaptive CFLmax < 0.9	Adaptive CFLmax < 0.9
Min/max time step (s)	0.074	–	0.035	0.012–0.07	0.05–0.14	0.10-0.20
# steps total (30 min)	24 324	–	51428	50 639	40 079	13 027
3D with ship						
# cells total	1477k	1477k	896k	–	645k	128k
Time step settings	Constant	Constant	Dynamic, outcome const.	–	Adaptive CFLmax<0.9	Adaptive CFLmax<0.9
Min/max time step (s)	0.078	0.078	0.035	–	0.00078–0.20	0.031-0.20
# steps total (30 min)	23 077	23 077	51 489	–	46866	19 015

Appendix A. Properties and settings of numerical codes

Tables 6 and 7 show the properties and settings of respectively the potential flow and coarse mesh CFD codes. All CFD codes are finite-volume codes with volume of fluid free-surface approximation. In OFA and OFA1, a 2nd-order implicit time integration (backward scheme) was used, and 2nd-order order spatial discretisation (with limited linear divergence scheme for convection). In OFB, a 1st-/2nd-order time integration blend was used (Crank–Nicolson 0.9), as well as a 1st-second order spatial discretisation blend (linear upwind and 2nd-order upwind with limiter), and a CMULES VOF scheme. This code used an adaptive time step, but the outcome was relatively constant. Still, the computational time for each time step varied because the number of outer iterations within each time step varied. Finally, in CF1-3, a first-order explicit time integration scheme was used, as well as first-order symmetry-preserving spatial discretisation. A PLIC-VOF with MACHO advection scheme was also used, and an absorbing boundary condition (GABC) at the outflow. Fig. 19 shows how the planes are defined through which the fluxes in direction of the ship's long axis were calculated with OFA, OFA1 and CF1-3.

Appendix B. Direct wave and ship response comparison

B.1. Undisturbed waves

The numerical wave results were compared to each other and to the experiments were possible. The largest wave crests in the example 3 h test 100504 at W1 and at COG are shown in Fig. 22, as well as the wave crest distributions. Scatter plots of reference versus predicted crests are also shown (using the matching procedure in Section 4.3). No experimental wave results are available at COG for the 3 h tests, so these results can only be compared between the different codes (PRE/FAT was taken as reference here). The OFA wave results were

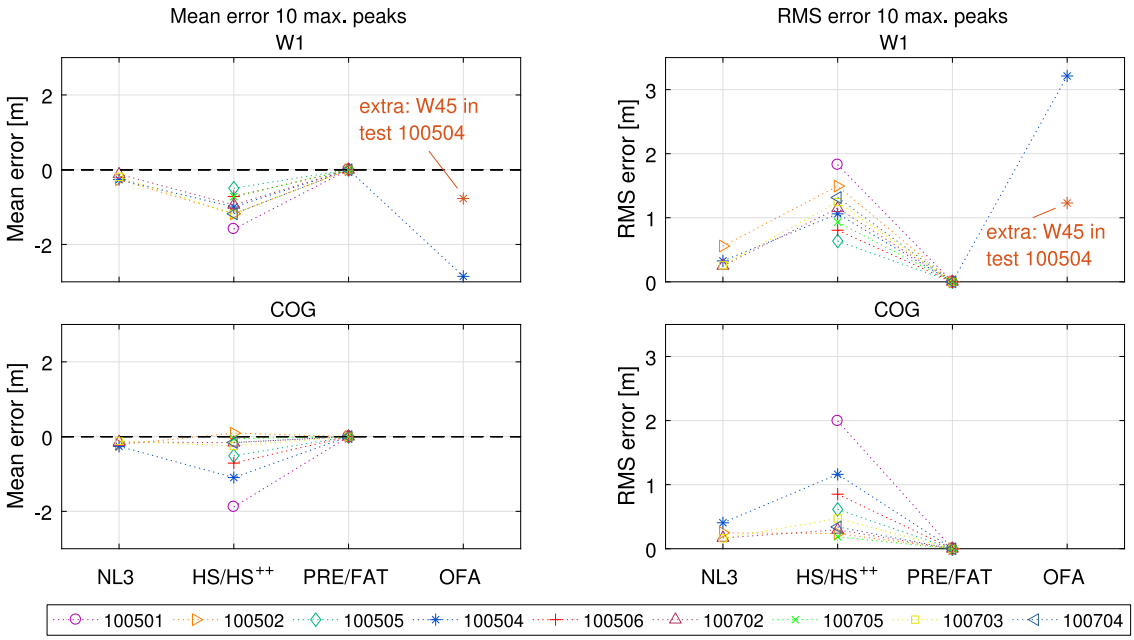

Fig. 20. All nine 3 h tests: mean and RMS error of the 10 highest undisturbed wave crests at W1 and COG (plus at W45 for OFA). Lead signal = EXP at W1 and PRE/FAT at COG (as EXP undisturbed waves are not available at COG).

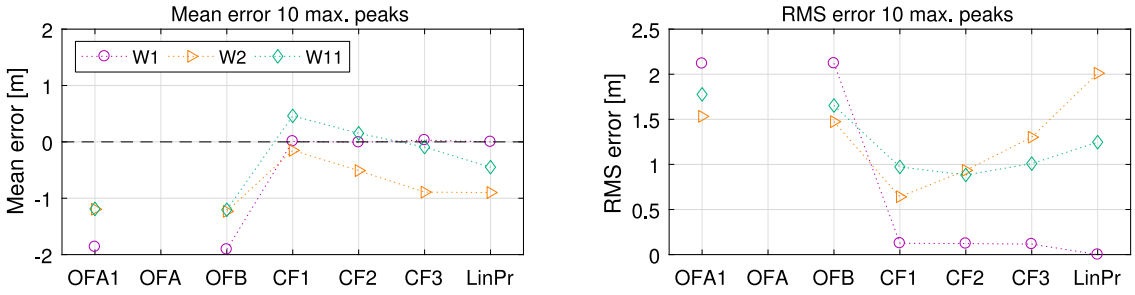

Fig. 21. 30 min run: mean and RMS error of the 10 highest undisturbed wave crests at W1, W2 and W11. Lead signal = EXP.

not delivered at the ship COG. Similar plots of the largest undisturbed wave crest, distribution and scatter at probe W11 for the single 30 min run 10050401 are shown in Fig. 23. Summary results for all 3 h tests at probe W1 and at COG are provided in Fig. 20, and for the 30 min run at probes W1, W2 and W11 in Fig. 21. These plots show the mean and root-mean-square (RMS) error for the 10 highest crests compared to the experiments for each test or run. For reference, the propagated wave using linear dispersion from W1 is also added to the 30 min plot (which of course is identical to the experiments at W1, hence zero error in Fig. 21 for signal 'LinPr' at W1). OFA did not deliver the undisturbed wave signals, so this signal is not visible in the 30 min figures.

The 3 h plots show that there are differences between the codes already in the input waves. The input waves were identical for HS/HS^{++}, and for PRE/FAT. HS/HS^{++} on average shows lower wave crests at COG than the other codes, especially for the larger wave crests. This is due to analytical post-processing of the experimental wave measurements (re-sampling, FFT component selection). As shown in Fig. 6, linear propagation from the wave probes to the COG was used for all potential flow codes, which will introduce similar errors compared to the real non-linear propagation of the steep wave conditions. The OFA results deviate much more from the experiments than the potential flow wave input. An important difference with the potential flow wave input is that these waves are the result of numerical wave propagation in the CFD code instead of analytical post-processing. This may have caused part of the wave quality loss. However, this is probably largely due to the choices made for the OFA wave input. Linear analytical wave elevation propagation from the experimental measurements at W45 to the inflow location was used, linear wave kinematics were added, after which the waves were propagated in the CFD code to the model and the other probes. The plots show that even the (re-)propagated result at W45 significantly deviates from the experiments.

The 30 min figures also show significant differences in waves at W11 between the coarse mesh CFD codes, especially for the higher wave crests. OFA1 and OFB are very similar and quite far below the experimental results for the highest wave crests, even though different ways were used to synthesise their input waves (Fig. 7). However, they both used linear wave propagation from another location to the inflow and a selection of the FFT components. By removing the higher-frequency components, the details of the steepest wave crests may have been removed. This is likely to be the main reason for the underestimation, although the wave handling in the code OpenFOAM could also contribute. The ComFLOW results on different grids show similar results with small mean errors for the highest crests, although grid 1 slightly overestimates them.

B.2. Ship response

Similar results are presented for the ship responses. The heave and pitch motions of the ship were delivered by all considered codes, as well as RWE at different probes (see Fig. 4). The largest peaks in RWE at RelBow are shown in Fig. 24 for 3 h test 100504, as well as the peak distributions and a scatter plot of matched peaks (using the zero

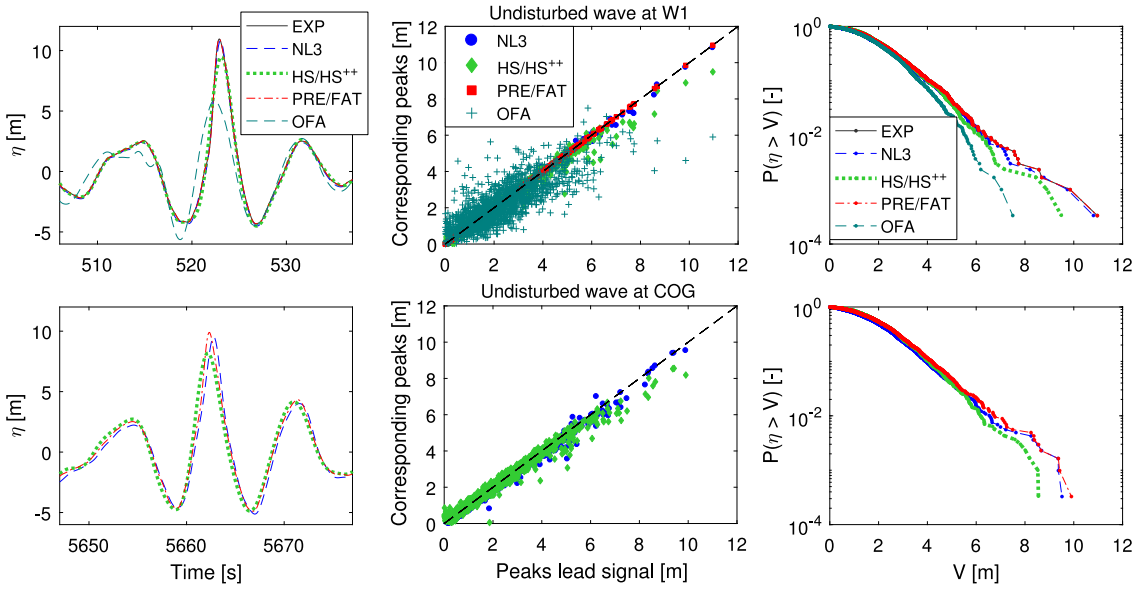

Fig. 22. Largest crest of undisturbed wave time traces at probes W1 and at COG and corresponding scatter plots and distributions of crests, 3 h test 100504. Lead signal = EXP at W1 and PRE/FAT at COG (as EXP undisturbed waves are not available at COG).

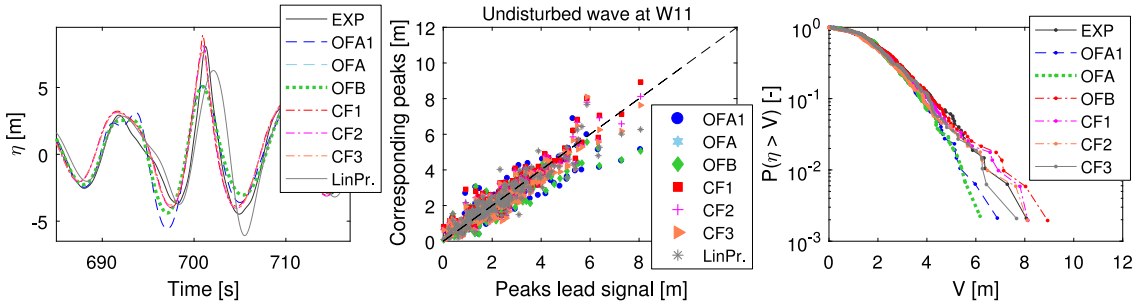

Fig. 23. Largest crest of undisturbed wave time traces at probe W11 (FPP of ship) and corresponding scatter plots and distributions of crests, 30 min run 10050401. Lead signal = EXP.

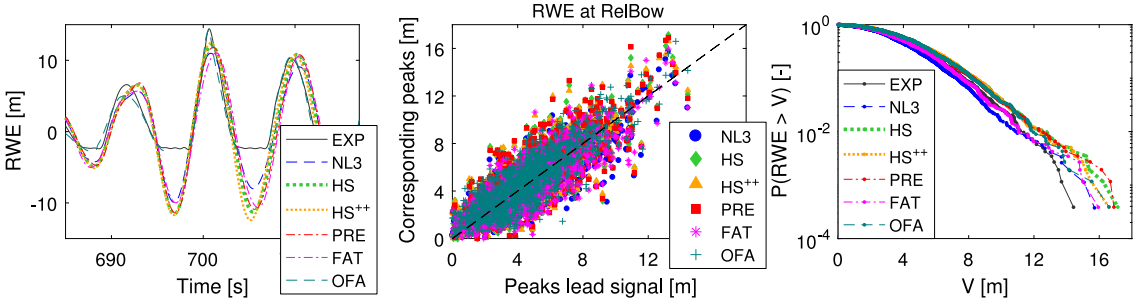

Fig. 24. Largest peaks in RWE at RelBow and corresponding scatter plots and distributions of peaks, 3 h test 100504. Lead signal = EXP.

up-crossing matching procedure in Section 4.3). Note that the experimental troughs are truncated due to the length of the probes. The mean and RMS error in the 10 largest peak values compared to the experiments are provided in Fig. 25 for all nine 3 h tests. It can be observed that the responses from all potential codes and OFA are relatively close to the experiments, but they are even closer to each other. There is no significant difference between the time- and frequency-domain codes, between the Rankine-source or zero speed Green's function codes or between linear and weakly non-linear codes. The OFA coarse mesh CFD result is also very close. The considered speeds are probably too low to show much better results with Rankine-source codes, and the motions are relatively small in the steep short waves, so the Froude–Krylov force components are also small. On average, both the heave and pitch motion peaks are overestimated compared to the experiments by all codes, with a large amount of scatter around the trends (more than in the incoming waves). This may be due to some small viscous damping effects in the experimental heave and pitch motions, that will be absent in potential flow and very small in CFD with a coarse mesh. The largest RWE peaks were slightly overestimated by all potential flow codes compared to the experiments. This may be due to water flowing over deck in the experiments, wave breaking that lowers RWE for the highest peaks and/or the overestimation of the numerical ship motions. The largest 10 RWE peaks have RMS errors around 2–3 m, which is significant compared to the H_s of 6.4–9.1 m.

Similar plots were made for 30 min run 10050401. Fig. 26 includes the heave, pitch and RWE results around the hull (similar as for the

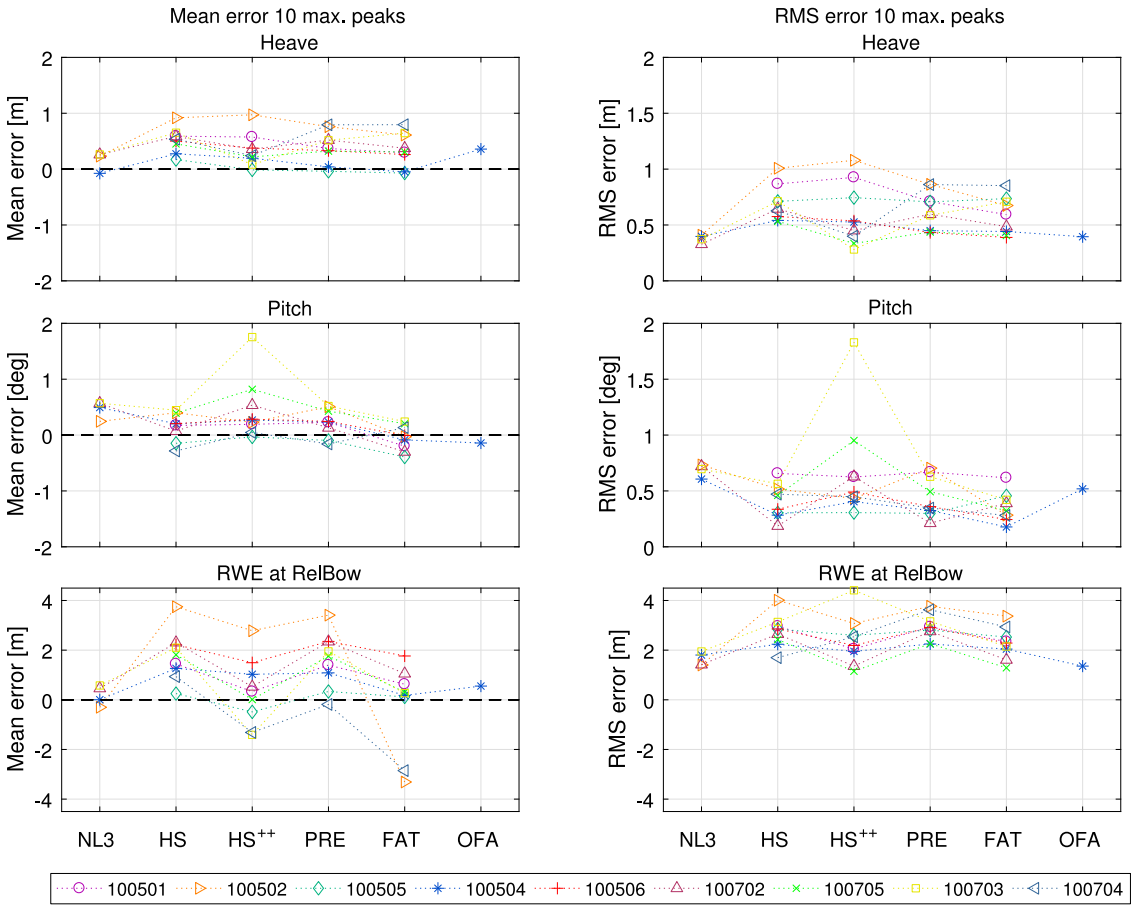

Fig. 25. All nine 3 h tests: mean and RMS error of the 10 highest peaks in motions (heave and pitch) and RWE (at RelBow). Lead signal = EXP.

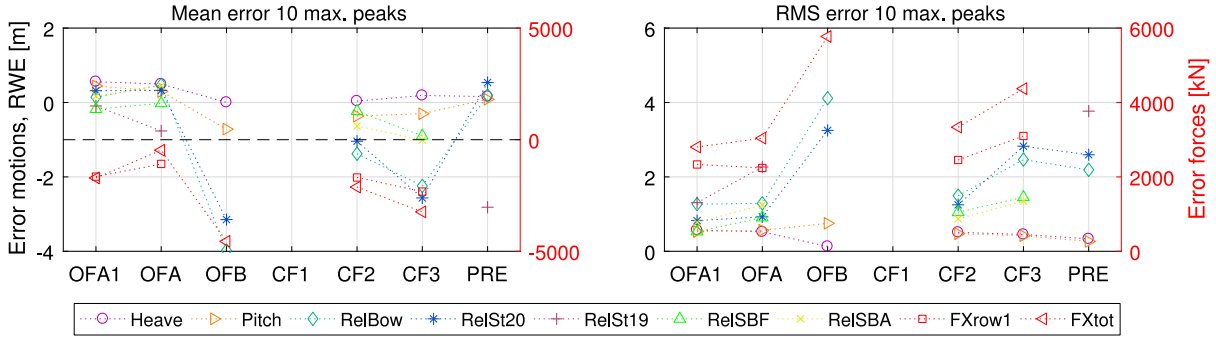

Fig. 26. 30 min run: mean and RMS error of the 10 highest peaks in motions (heave and pitch), RWE (at three locations) and coarse mesh breakwater force (bottom row of panels and total breakwater). Lead signal = EXP.

3 h tests), but also the RWE on deck and coarse mesh CFD forces on the breakwater. Results of CF1 were not delivered with the ship (only for the undisturbed waves). The RWE on deck, coarse mesh force on the bottom row and fluxes were not delivered by OFB. As there is no experimental result for the fluxes through planes on deck (Fig. 19), the error plot of this signal is omitted. Similar as for the potential flow and OFA results discussed above, the mean heave and pitch peaks from all coarse mesh CFD calculations were over-predicted compared to the experiments. This is not very surprising, as effects of viscous damping in the motions are also underestimated by CFD on a coarse mesh. The 30 min mean and RMS errors of the 10 largest motion and RWE peaks in Fig. 26 are also very similar to those based on the 3 h potential flow results for head waves (all tests starting with 1005) in Fig. 25. This indicates that the coarse mesh CFD screening results were not expected to be much better than the potential flow screening results. On the other hand, the extra indicators such as wave elevation on deck, forces and fluxes that CFD can produce may also be valuable indicators. The coarse mesh force on the breakwater was expected to deviate significantly from the experimental results. This is also visible in Fig. 26. Still, the order of the peaks can be an efficient green water indicator (see Section 5).

Appendix C. Extra 3 h indicator scatter plots

The present appendix shows other 3 h scatter plots for the matched indicator and force peaks. The main text includes these plots for one example test (100504) and two indicators (peaks in RelSt19 and crests in W11). Plotting all combinations of indicators and tests is too elaborate, but Fig. 27 shows the scatters for the other considered indicators for

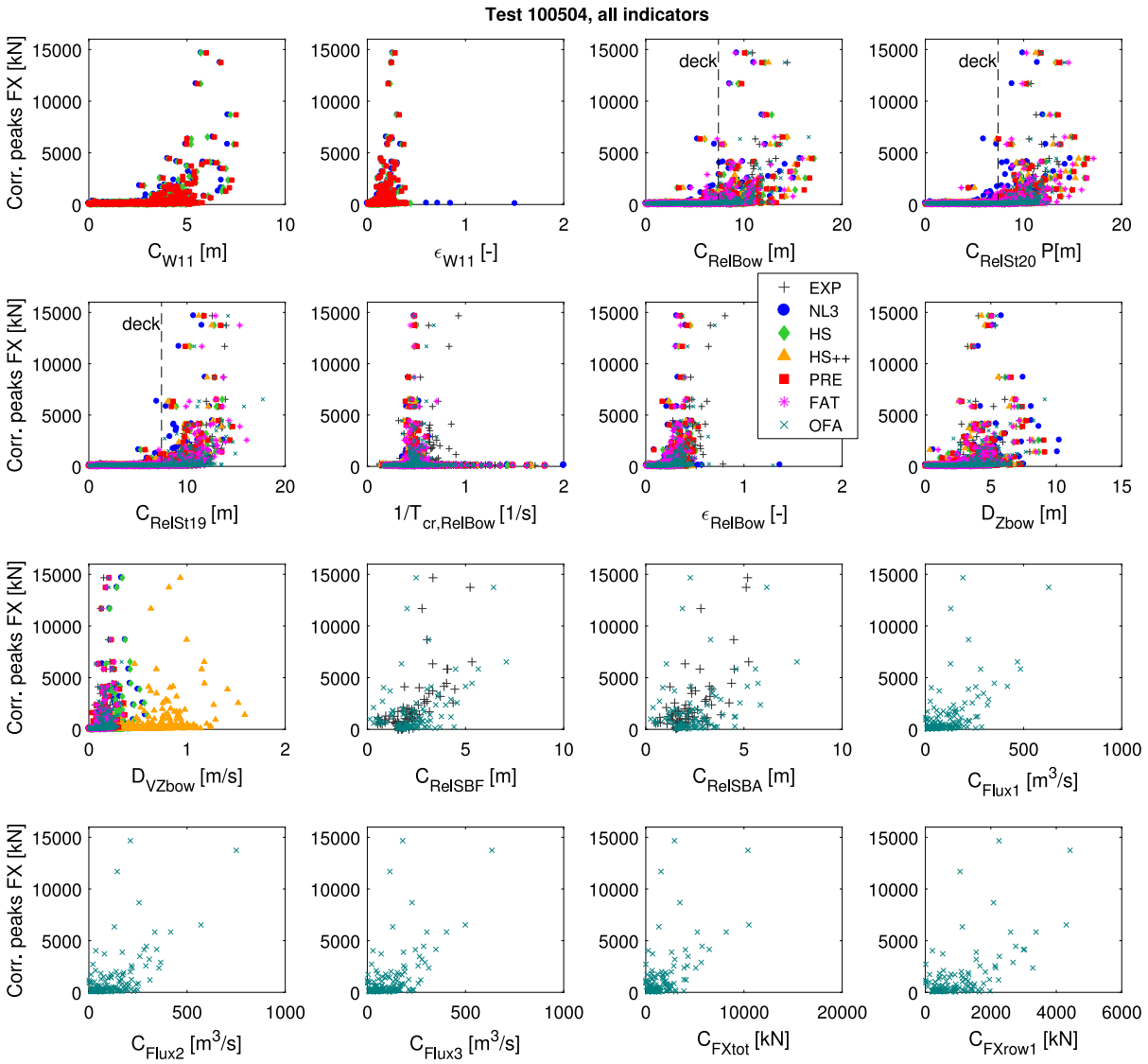

Fig. 27. Scatter plots indicator versus force peaks, example test 100504, all indicators (where C = crests, D = troughs, T_{cr} = rise times, ϵ = crest front steepness).

test 100504, and Figs. 28 and 29 show the same for the two example indicators in all 3 h test conditions.

Appendix D. Example impacts

This appendix describes a few selected example impacts that determine outliers in SQI for indicator peaks in RWE at the bow. High-speed video recordings are shown when available, otherwise snapshots from the normal video recording are shown.

Event 1 in head wave test 100506 determines the SQI for RelBow at the lower force thresholds (Fig. 30). It shows a relatively high force (4800 kN), for a relatively low RWE (~9 m). The figure shows that all potential flow codes correspond well to the experimental result, so the quality of the response prediction is not the problem. The snapshots show that this elevation indeed was limited. This is especially the case at the bow, RelSt19 serves as better indicator for this particular event. A sheet of water moves to two sides of the bow, which does not lead to loading on the breakwater. However, a high-speed jet of water also moves over the middle of the fore deck, impacting the breakwater. This jet was formed by water that just exceeded the freeboard. The first snapshot shows that the incoming wave for this event is quite high and steep, just before breaking. The horizontal kinematics of the water in the crest, just overtopping the freeboard, may well cause the jet over the fore deck. This type of event is hard to predict using linear or even non-linear RWE; using non-linear horizontal wave velocities as indicators could maybe improve this. The event is an outlier in the peaks of RelBow SQI, but it is an event that indeed cannot be accurately predicted by this indicator.

Event 2 was found in head wave test 100504 (but not in run 1 that was evaluated as 30 min run), see Fig. 31. The potential flow RWE for this event are low, whereas the force on the breakwater is considerable (~6000 kN). The time traces show that the experimental and OFA results are much higher than the potential flow results for this event. This points in the direction of a non-linear steep wave event, which is confirmed by the snapshots. Increasing the non-linearity in the incoming wave component of the RWE will probably significantly improve the potential flow screening results in this case; they could get closer to the experimental and OFA results.

Event 3 was found in bow-quartering test 100703 (Fig. 32). This bow-quartering test was one of the most difficult conditions to screen for all codes, but especially for HS^{++}. The figure highlights an event where all other codes perform consistently. It shows that HS^{++} does not predict a high RWE peak for this event, and the time trace appears differently from the others. The other codes are quite similar to each other and to the experiments around this time. Inspection of the time traces showed that this is the case more often for HS^{++} in this test, but

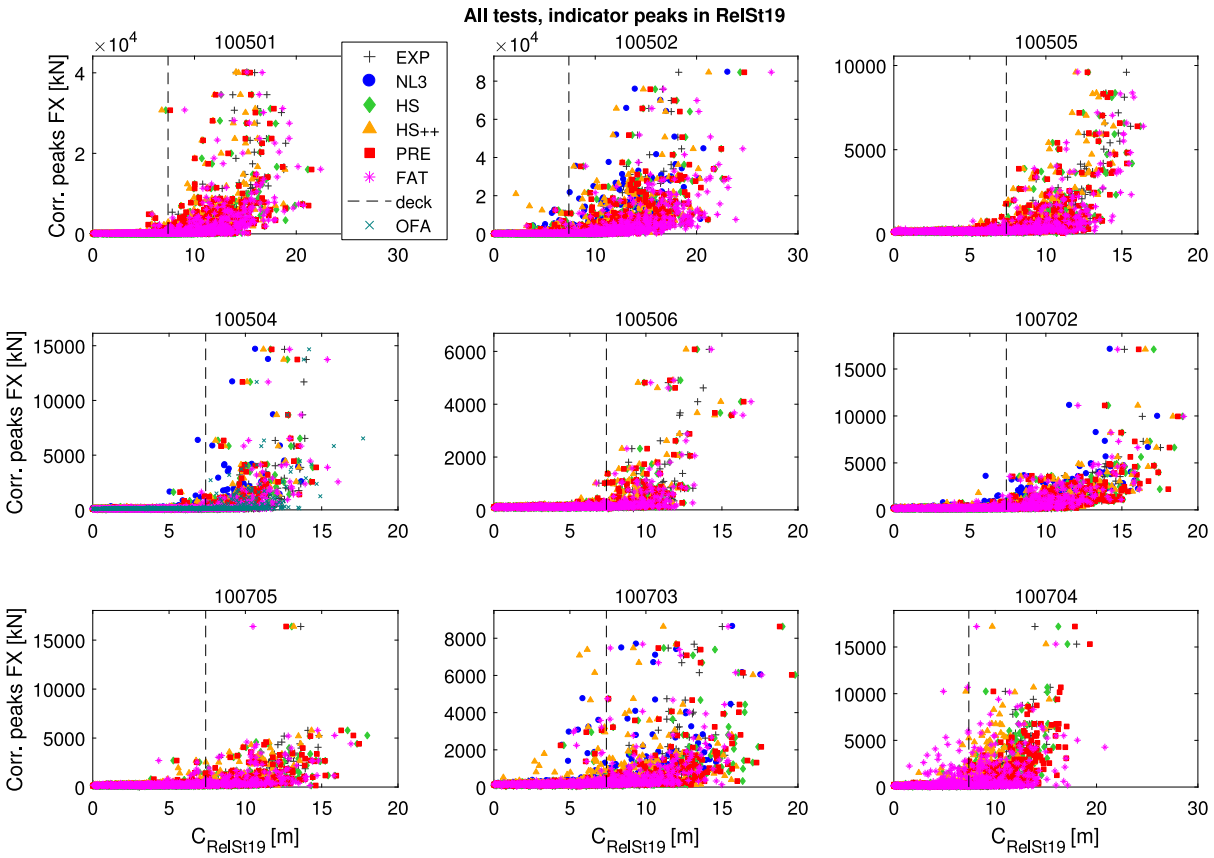

Fig. 28. Scatter plots indicator versus force peaks, all tests, indicator peaks RelSt19 (where C = crests).

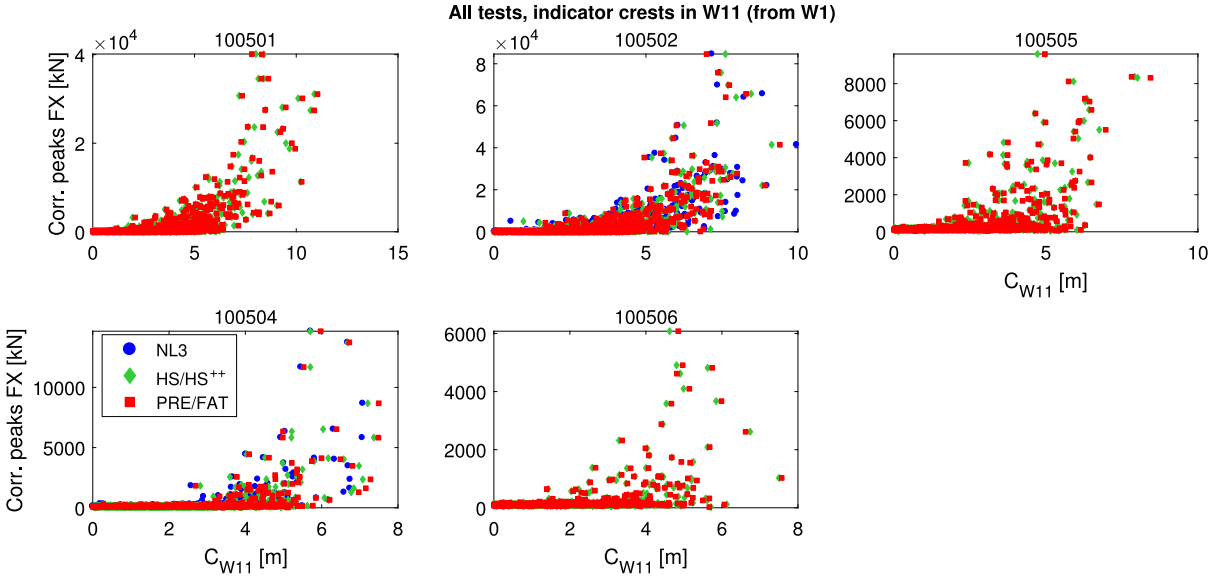

Fig. 29. Scatter plots indicator versus force peaks, all head wave tests, indicator crests W11 from W1 (where C = crests).

not all the time. The erratic behaviour is not explained by the wave input, as that would lead to similar results from HS. This is not the case, the HS time trace matches the other codes well. It is therefore due to something in the HS^{++} code.

Event 4 was the largest event in bow-quartering test 100704 (Fig. 33). The RWE at the bow predicted for this event serve reasonably well as indicator; but there is quite some variation between the codes in the scatter plot. Part of this is caused by the differences in wave input discussed earlier. For instance all differences between PRE and HS should be attributed to this, as the codes are very similar. However, the wave input for HS and HS^{++} was identical, so there are also differences due to the codes. This condition is the most difficult one, with a

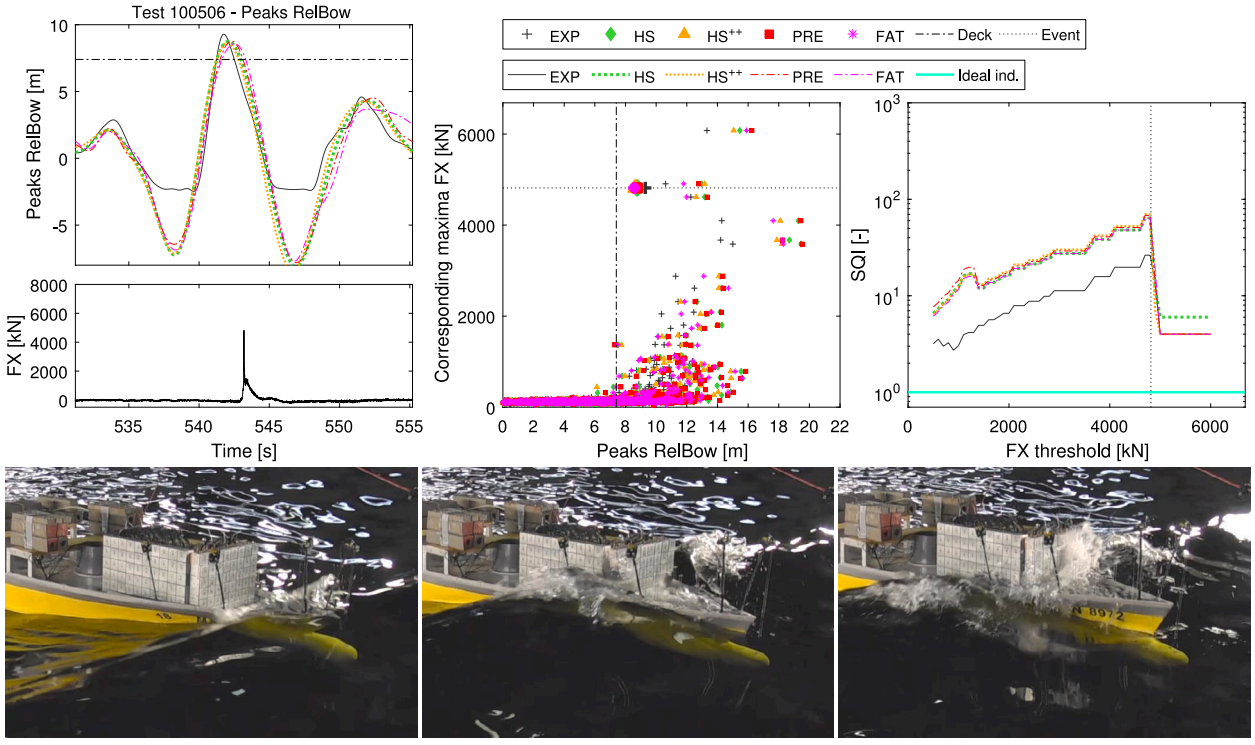

Fig. 30. Example event 1 in test 100506 (μ 180 deg, H_s 6.4 m, T_p 12.1 s, V_x 5 kn): indicator peak, force peak, scatter plot (with selected event in larger markers), screening quality plot and snapshots.

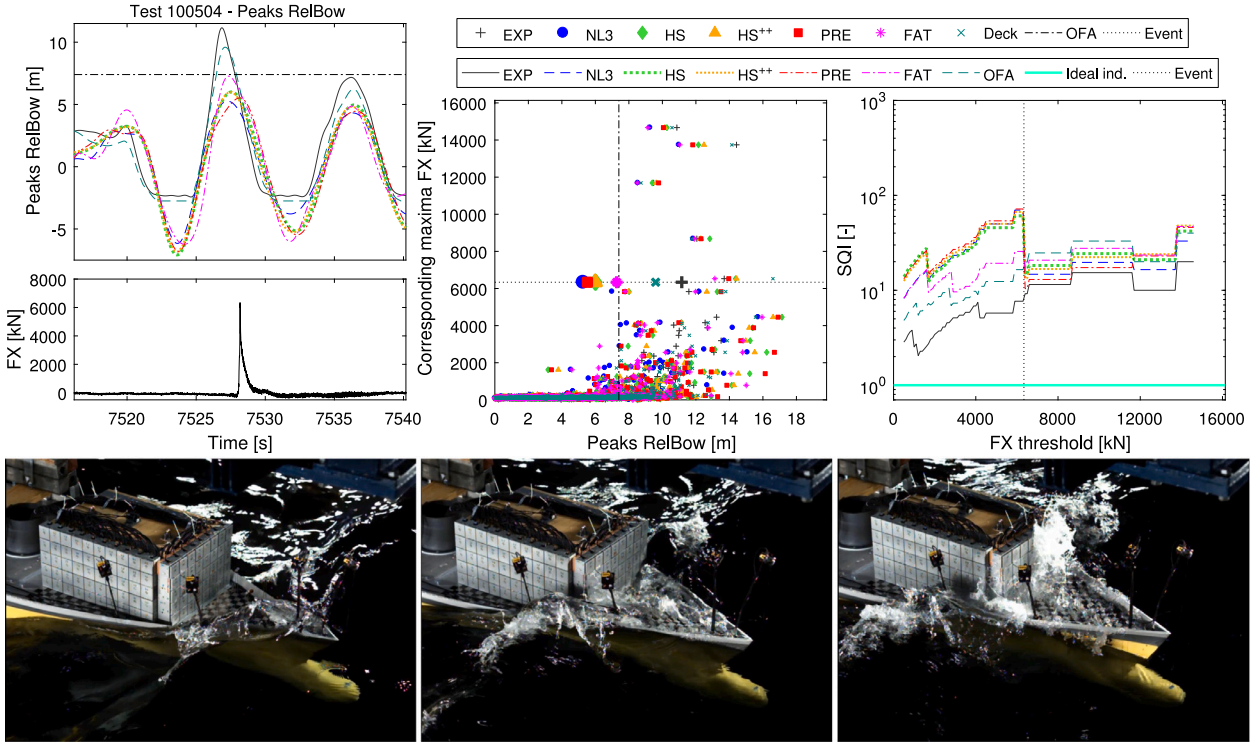

Fig. 31. Example event 2 in test 100504 (μ 180 deg, H_s 6.8 m, T_p 9.7 s, V_x 5 kn): indicator peak, force peak, scatter plot (with selected event in larger markers), screening quality plot and snapshots.

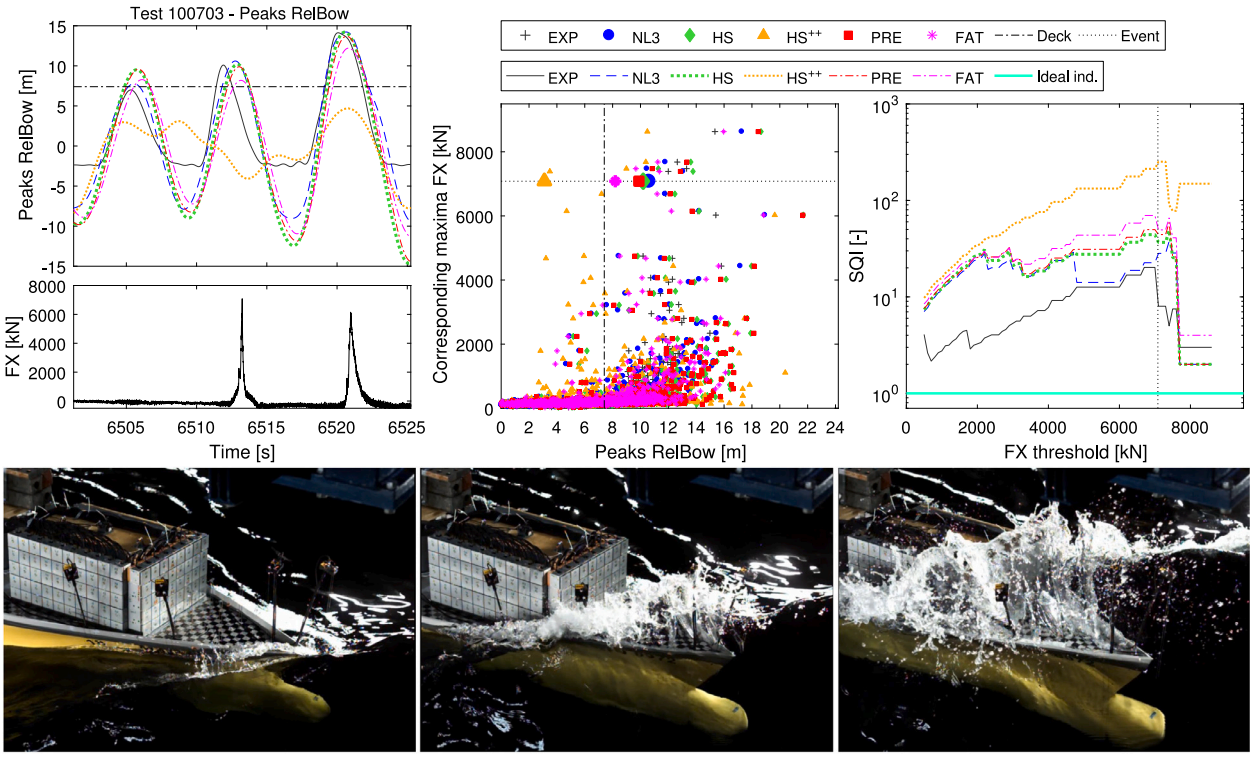

Fig. 32. Example event 3 in test 100703 (μ 135 deg, H_s 7.0 m, T_p 9.7 s, V_x 5 kn): indicator peak, force peak, scatter plot (with selected event in larger markers), screening quality plot and snapshots.

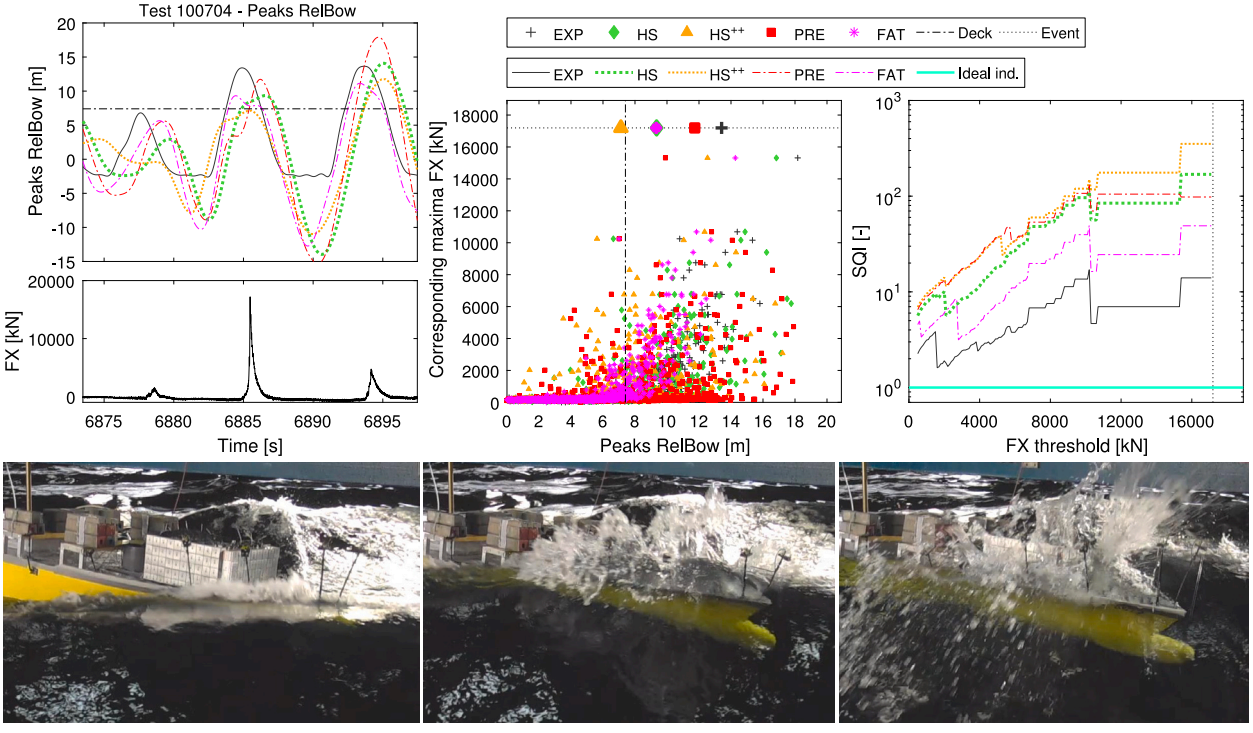

Fig. 33. Example event 4 in test 100704 (μ 135 deg, H_s 6.8 m, T_p 9.7 s, V_x 10 kn): indicator peak, force peak, scatter plot (with selected event in larger markers), screening quality plot and snapshots.

relatively high forward speed of 10 kn in a severe bow-quartering wave condition. Considering that, the potential flow screening still performs relatively well. The snapshots show that this event is associated with a breaking wave just in front of the model. The introduced non-linearity is included in the experimental RWE, but not in the potential flow results. Including some non-linearity in the indicator may therefore improve the results.

References

ABS, 2013. User guide for ABS eagle seakeeping, version 2.0b.

Adegeest, L., Braathen, A., Løseth, R., 1998. Use of nonlinear sea loads simulations in design of ships. In: 12th Int. Conf. on Practical Design of Ships and Other Floating Structures (PRADS). The Hague, The Netherlands, pp. 53–58.

Bales, N.K., 1977. Slamming and deck wetness characteristics of a United States Coast Guard medium endurance cutter (WMEC) in long-crested head seas. Report, David Taylor Naval Ship Research and Development Center, Bethesda, USA.

Bandringa, H., Helder, J., 2018. On the validity and sensitivity of CFD simulations for a deterministic breaking wave impact on a semi submersible. In: 37th Int. Conf. on Ocean, Offshore and Arctic Eng. (OMAE). ASME, Madrid, Spain, http://dx.doi.org/10.1115/OMAE2018-78089.

Bandringa, H., Helder, J., van Essen, S.M., 2020. On the validity of CFD for simulating extreme green water loads on ocean-going vessels. In: 39th Int. Conf. on Ocean, Offshore and Arctic Eng. (OMAE). ASME, Virtual, Online, http://dx.doi.org/10.1115/OMAE2020-18290.

Benhamou, A., Seng, S., Monroy, C., Lauzon, J.D., Malenica, S., 2018. Hydroelastic simulations in OpenFOAM: a case study on a 4400TEU containership. In: 8th Int. Conf. on Hydroelasticity in Marine Technology. SNU, Seoul, Korea.

Bøckmann, A., Gramstad, O., Helmers, J.B., Lande, Ø., 2018. Realistic design waves for wave-in-deck problems. In: 37th Int. Conf. on Ocean, Offshore and Arctic Eng. (OMAE). ASME, Madrid, Spain, http://dx.doi.org/10.1115/OMAE2018-78411.

Bogaert, H., 2018. An experimental investigation of sloshing impact physics in membrane LNG tanks on floating structures (Ph.D. thesis). Delft University of Technology, Delft, The Netherlands, http://dx.doi.org/10.4233/uuid:96870b88-e07b-4ec2-8bd4-ef2cd3713568.

Buchner, B., 1994. On the effect of green water impacts on ship safety (a pilot study). In: Int. Conf. on Ship and Marine Research. NAV, Rome, Italy.

Buchner, B., 2002. Green water on ship-type offshore structures (Ph.D. thesis). Delft University of Technology, Delft, The Netherlands.

Buchner, B., van den Berg, J., Helder, J., Bunnik, T.H.J., 2014. Non-linear wave runup along the side of ships causing green water problems: experiments and first CFD calculations. In: 33rd Int. Conf. on Ocean, Offshore and Arctic Eng. (OMAE). ASME, San Francisco, USA, http://dx.doi.org/10.1115/OMAE2014-23022.

Buchner, B., van Dijk, R., Voogt, A., 2007. The spatial analysis of an extreme wave in a model basin. In: 26th Int. Conf. on Ocean, Offshore and Arctic Eng. (OMAE). ASME, San Diego, USA, http://dx.doi.org/10.1115/OMAE2007-29409.

Bunnik, T.H.J., 1999. Seakeeping calculations for ships, taking into account the non-linear steady waves (Ph.D. thesis). Delft University of Technology, Delft, The Netherlands.

Bunnik, T.H.J., Scharnke, J., de Ridder, E.J., 2019. Efficient indicators for screening of random waves for wave impacts on a jacket platform and a fixed offshore wind turbine. In: 38th Int. Conf. on Ocean, Offshore and Arctic Eng. (OMAE). ASME, Glasgow, UK, http://dx.doi.org/10.1115/OMAE2018-95481.

Bunnik, T.H.J., Stansberg, C.T., Pakozdi, C., Fouques, S., Somers, L., 2018. Useful indicators for screening of sea states for wave impacts on fixed and floating platforms. In: 37th Int. Conf. on Ocean, Offshore and Arctic Eng. (OMAE). ASME, Madrid, Spain, http://dx.doi.org/10.1115/OMAE2018-78544.

Derbanne, Q., de Hauteclocque, G., 2019. A new approach for environmental contour and multivariate de-clustering. In: 38th Int. Conf. on Ocean, Offshore and Arctic Eng. (OMAE). ASME, Glasgow, UK, http://dx.doi.org/10.1115/OMAE2019-95993.

Dietz, J.S., 2004. Application of conditional waves as critical wave episodes for extreme loads on marine structures (Ph.D. thesis). Technical University of Denmark, Lyngby, Denmark.

Dietz, J.S., Hansen, P.F., Jensen, J.J., 2004. Design wave episodes for extreme value ship responses. In: 9th Int. Conf. on Practical Design of Ships and Other Floating Structures (PRADS), Hamburg, Germany.

DNV, 2010. Recommended practice DNV-RP-C205: environmental conditions and environmental loads. Det Norske Veritas, Oslo, Norway.

Eggers, R., Gaillarde, G., Koning, J., 2012. A review of unsteady hydrodynamic behaviour of sailing yachts and methods to study it. In: 4th High Performance Yacht Design Conf.. Charterworld, Auckland, New Zealand.

Ersdal, G., Kvitrud, A., 2000. Green water on Norwegian production ships. In: 10th ISOPE Conf.. Int. Society of Offshore and Polar Eng., Seattle, USA.

van Essen, S.M., 2019. Variability in encountered waves during deterministically repeated seakeeping tests at forward speed. In: 38th Int. Conf. on Ocean, Offshore and Arctic Eng. (OMAE). ASME, Glasgow, UK, http://dx.doi.org/10.1115/OMAE2019-95065.

van Essen, S.M., 2021. Influence of wave variability on ship response during deterministically repeated seakeeping tests at forward speed. In: 14th Int. Conf. on Practical Design of Ships and Other Floating Structures (PRADS, Yokohama, Japan, 2019). In: Lecture Notes on Civil Eng., vol. 63, Springer Nature Singapore, pp. 899–925. http://dx.doi.org/10.1007/978-981-15-4624-2_54.

van Essen, S.M., Bandringa, H., Helder, J., Buchner, B., 2020a. Non-linear wave run-up along the side of sailing ships causing green water on deck: experiments and deterministic calculations. In: 39th Int. Conf. on Ocean, Offshore and Arctic Eng. (OMAE). ASME, Virtual, Online, http://dx.doi.org/10.1115/OMAE2020-18130.

van Essen, S.M., Scharnke, J., Bunnik, T.H.J., Düz, B., Bandringa, H., Hallmann, R., Helder, J., 2020b. Linking experimental and numerical wave modelling. J. Mar. Sci. Eng. 8, 198. http://dx.doi.org/10.3390/jmse8030198.

Friis-Hansen, P., Nielsen, L.P., 1995. On the New Wave model for the kinematics of large ocean waves. In: 14th Int. Conf. on Ocean, Offshore and Arctic Eng. (OMAE). ASME, Copenhagen, Denmark.

Ge, Z., Shen, Z., Yan, D., Chien, H.P., 2018. CFD-Predicted slamming loads on a ship in head and oblique seas. In: 32nd Symp. on Naval Hydrodynamics. TUHH, Hamburg, Germany.

Grin, R., van Heerd, J., Ferrari, V., 2013. Hydrodynamic aspects in the design of passenger vessels. In: Int. Conf. on Design and Operation of Passenger Ships. RINA, London, UK.

Haver, S., Kleiven, G., 2004. Environmental contour lines for design purposes - why and when?. In: 23rd Int. Conf. on Ocean, Offshore and Arctic Eng. (OMAE). ASME, Vancouver, Canada, http://dx.doi.org/10.1115/OMAE2004-51157.

Haver, S., Winterstein, S.R., 2008. Environmental contour lines: a method for estimating long term extremes by a short term analysis. In: SNAME Annual Meeting. Society of Naval Architects and Marine Engineers, Houston, USA.

Hennig, J., Scharnke, J., Swan, C., Hagen, Ø., Ewans, K., Tromans, P.S., Forristall, G., 2015. Effect of short-crestedness on extreme wave impact - a summary of findings from the joint industry project "ShorTCresT". In: 34th Int. Conf. on Ocean, Offshore and Arctic Eng. (OMAE). ASME, St. John's, Canada, http://dx.doi.org/10.1115/OMAE2015-41167.

Jacobsen, N.G., Fuhrman, D.R., Fredsøe, J., 2012. A wave generation toolbox for the opensource CFD library OpenFOAM. Int. J. Numer. Methods Fluids 70 (9), 1073–1988. http://dx.doi.org/10.1002/fld.2726.

Johannessen, T.B., Hagen, Ø., 2012. Estimating design levels for strongly nonlinear response. In: 31st Int. Conf. on Ocean, Offshore and Arctic Eng. (OMAE). ASME, Rio de Janeiro, Brazil, http://dx.doi.org/10.1115/OMAE2012-83947.

Johannessen, T.B., Lande, Ø., 2018. Long term analysis of steep and breaking wave properties by event matching. In: 37th Int. Conf. on Ocean, Offshore and Arctic Eng. (OMAE). ASME, Madrid, Spain, http://dx.doi.org/10.1115/OMAE2018-78283.

Kapsenberg, G.K., 2018. On the slamming of ships (Ph.D. thesis). Delft University of Technology, Delft, The Netherlands, http://dx.doi.org/10.4233/uuid:14eac2bb-63ee-47e4-8218-1ba3830a97b4.

Kawamura, K., Hashimoto, H., Matsuda, A., Terada, D., 2016. SPH Simulation of ship behaviour in severe water-shipping situations. J. Ocean Eng. 120, 220–229. http://dx.doi.org/10.1016/j.oceaneng.2016.04.026.

Kim, D.-H., 2012. Design loads generator: estimation of extreme environmental loadings for ship and offshore applications (Ph.D. thesis). University of Michigan, Ann Arbor, USA.

Kim, D.-H., Engle, A.H., Troesch, A.W., 2012. Estimates of long-term combined wave bending and whipping for two alternative hull forms. Trans. SNAME 120.

Kim, D.-H., Troesch, A.W., 2014. Statistical estimation of extreme roll responses in short crested irregular head seas. Trans. SNAME 122.

Lindgren, G., 1970. Some properties of a normal process near a local maximum. Ann. Math. Stat. 41 (6), http://dx.doi.org/10.1214/aoms/1177696688.

Luppes, R., van der Heiden, H.J.L., van der Plas, P., Düz, B., 2013. Simulations of wave impact and two-phase flow with ComFLOW: past and recent developments. In: 19th ISOPE Conf.. Int. Society of Offshore and Polar Eng., Anchorage, USA.

Myrhaug, D., Kjeldsen, S., 1986. Steepness and asymmetry of extreme waves and the highest waves in deep water. J. Ocean Eng. 13, 549–568. http://dx.doi.org/10.1016/0029-8018(86)90039-9.

Nielsen, K.B., 2003. Numerical prediction of green water loads on ships (Ph.D. thesis). Technical University of Denmark, Lyngby, Denmark.

Ochi, M.K., 1964a. Extreme behavior of a ship in rough seas. In: Annual Meeting. Society of Naval Architects and Marine Engineers, London, UK, pp. 143–202.

Ochi, M.K., 1964b. Prediction of occurrence and severity of ship slamming at sea (ACR112). In: 5th Symp. on Naval Hydrodynamics. Office of Naval Research, Bergen, Norway.

Ogawa, Y., Minumi, M., Tunizuwu, K., Kumuno, A., Mutsunami, R., Huyushi, T., 2002. Shipping water load due to deck wetness. In: 12th ISOPE Conf.. Int. Society of Offshore and Polar Eng., Kitayushu, Japan.

Oger, G., Ducrozet, G., Touzé, D.L., Candelier, J., ad Guilcher, P.M., 2014. A coupled SPH-spectral method for the simulation of wave train impacts on a fpso. In: 33rd Int. Conf. on Ocean, Offshore and Arctic Eng. (OMAE). ASME, San Francisco, USA, http://dx.doi.org/10.1115/OMAE2014-24679.

Pákozdi, C., Ostman, A., Stansberg, C.T., Fonseca, D., de Carvalho e Silva, D.F., 2014. Green water on FPSO analyzed by a coupled potential-flow NS-VOF method. In: 33rd Int. Conf. on Ocean, Offshore and Arctic Eng. (OMAE). ASME, San Francisco, USA, http://dx.doi.org/10.1115/OMAE2014-23913.

Pastoor, L.W., 2002. On the assessment of nonlinear ship motions and loads (Ph.D. thesis). Delft University of Technology, Delft, The Netherlands.

Scharnke, J., 2019. Elementary loading processes and scale effects involved in wave-in-deck type of loading - a summary of the BreaKin JIP. In: 38th Int. Conf. on Ocean, Offshore and Arctic Eng. (OMAE). ASME, Glasgow,UK, http://dx.doi.org/10.1115/OMAE2019-95004.

Seyffert, H.C., 2018. Extreme design events due to combined non-Gaussian loading (Ph.D. thesis). University of Michigan, Ann Arbor, USA.

Seyffert, H.C., Kana, A.A., Troesch, A.W., 2020. Numerical investigation of response-conditioning wave techniques for short-term rare combined loading scenarios. J. Ocean Eng. 213, 107719. http://dx.doi.org/10.1016/j.oceaneng.2020.107719.

Seyffert, H.C., Kana, A.A., Troesch, A.W., 2021. Design contours for complex marine systems. In: 14th Int. Conf. on Practical Design of Ships and Other Floating Structures (PRADS, Yokohama, Japan, 2019). In: Lecture Notes on Civil Eng., vol. 64, Springer Nature Singapore, pp. 168–183. http://dx.doi.org/10.1007/978-981-15-4672-3_10.

Sharma, J.N., Dean, R.G., 1979. Development and evaluation of a procedure for simulating a random directional second order sea surface and associated wave forces. Ocean Eng. Report 20, University of Delaware, Newark.

Shen, Z., Hsieh, Y.F., Ge, Z., Korpus, R.A., Huan, J., 2016. Slamming load prediction using overset CFD methods (OTC-27254-MS). In: Offshore Technology Conf.. OTC, Houston, USA.

Shen, Z., Korpus, R.A., 2015. Numerical simulations of ship self-propulsion and maneuvering using dynamic overset grids in OpenFOAM. In: A Workshop on CFD in Ship Hydrodynamics. NMRI, Tokyo, Japan.

SIMMAN, 1997. KCS Geometry. http://www.simman2008.dk/KCS/container.html (Accessed: 28 January 2021).

Stansberg, C.T., 1998. Non-Gaussian extremes in numerically generated second-order random waves on deep water. In: 8th ISOPE Conf.. Int. Society of Offshore and Polar Eng., Montreal, Canada.

Stansberg, C.T., 2008. A wave impact parameter. In: 27th Int. Conf. on Ocean, Offshore and Arctic Eng. (OMAE). ASME, Estoril, Portugal, http://dx.doi.org/10.1115/OMAE2008-57801.

Stansberg, C.T., 2020. Wave front steepness and influence on horizontal deck impact loads. J. Mar. Sci. Eng. 8, 314, http://dx.doi.org/10.3390/jmse8050314.

Taylor, P.H., Jonathan, P., Harland, L.A., 1997. Time domain simulation of jack-up dynamics with the extremes of a Gaussian process. J. Vib. Acoust. 119, 624–628. http://dx.doi.org/10.1115/1.2889772.

Torhaug, R., 1996. Extreme response of nonlinear ocean structures: identification of minimal stochastic wave input for time-domain simulation. Stanford University, California, USA.

Tromans, P.S., Anaturk, A.R., Hagemeijer, P., 1991. A new model for the kinematics of large ocean waves - application as a design wave. In: 1st ISOPE Conf.. Int. Society of Offshore and Polar Eng., Edinburgh, UK, pp. 64–71.

van 't Veer, A.P., Vlasveld, E., 2014. Green water phenomena on a twin-hull FLNG concept. In: 33rd Int. Conf. on Ocean, Offshore and Arctic Eng. (OMAE). ASME, San Francisco, USA, http://dx.doi.org/10.1115/OMAE2014-23915.

Voogt, A., Buchner, B., 2004. Prediction of wave impact loads on ship-type offshore structures in steep fronted waves (JSC-343). In: 14th ISOPE Conf.. Int. Society of Offshore and Polar Eng., Toulon, France.

Winterstein, S.R., Ude, T.C., Cornell, C.A., Bjerager, P., Haver, S., 1993. Environmental parameters for extreme response: inverse FORM with omission factors. In: Int. Conf. on Structural Safety and Reliability (ICOSSAR), Innsbruck, Austria.